AN ABSTRACT OF THE THESIS OF

Bradley A. Ling for the degree of Master of Science in Mechanical Engineering presented on June 9, 2015.

Title: Real-Time Estimation and Prediction of Wave Excitation Forces for Wave Energy Control Applications

Abstract approved: _____

Belinda A. Batten

Wave energy is emerging as a new potential source for renewable energy generation. However, wave energy technology is not currently cost competitive with other more mature renewable energy sources such as wind and solar. One approach that researchers and developers are taking to reduce the cost of wave energy is to actively control wave energy converters (WECs) in such a way that the average power produced by the WEC is significantly increased. Most of the proposed control algorithms depend on having predictions of the future wave forces, as the optimal control actions depend on these future forces.

This thesis details a methodology that uses a Kalman filter to estimate the wave forces on a WEC from measured motions of a WEC in real-time. These estimated forces are then used to predict future forces with a recursive, autoregressive least squares prediction model. The methodology is tested on a generic, 3 degree of freedom, point absorbing WEC in simulations, using recorded water surface elevation time series data as input to the WEC model. The effect of different sea states on both estimation and prediction accuracies is investigated. Results show that both estimation and prediction accuracies depend on the hydrodynamic properties of the WEC. It is also observed that low energy sea states result in significantly reduced estimation and prediction accuracies compared to more energetic sea states.

Real-Time Estimation and Prediction of Wave Excitation Forces for Wave Energy Control Applications

by

Bradley A. Ling

A THESIS

submitted to

Oregon State University

in partial fulfillment of
the requirements for the
degree of

Master of Science

Presented June 9, 2015
Commencement June 2015

Master of Science thesis of Bradley A. Ling presented on June 9, 2015.

APPROVED:

_____

Major Professor, representing Mechanical Engineering

_____

Head of the School of Mechanical, Industrial, and Manufacturing Engineering

_____

Dean of the Graduate School

I understand that my thesis will become part of the permanent collection of Oregon State University libraries. My signature below authorizes release of my thesis to any reader upon request.

_____

Bradley A. Ling, Author

ACKNOWLEDGEMENTS

I would like to thank my advisor Dr. Belinda Batten for your support and guidance throughout my time at Oregon State. You have been the best advisor a graduate student could ask for. I also want to thank all of the other professors that have helped me throughout my studies, especially Dr. Robert Paasch for your continued involvement in the marine renewable energy research at OSU. You have all had a positive impact on my education.

For all of my fellow graduate students, it has been a pleasure working beside you. The conversations about marine renewable energy, coursework, bicycle maintenance, and many other topics proved to be invaluable. I wish you all the best of luck going forward.

I want to thank my family for their endless love and support. Without you, I would not be where I am today. Last but not least thank you Tiegen for your persistent love and the sacrifices you have made to support my dream of attending graduate school. I couldn't have done it without you.

TABLE OF CONTENTS

TABLE OF CONTENTS (Continued)

LIST OF FIGURES

LIST OF FIGURES (Continued)

LIST OF TABLES

To my grandfather Robert J. Bayer for inspiring me to pursue a career in engineering.

Chapter 1: Introduction

Interest in wave energy has increased as our society strives to increase renewable energy sources. It has been estimated that wave energy could contribute 470 TWh/year of power annually for the continental United States, which is approximately 12% of total U.S. electricity usage [1]. Wave energy has a few potential benefits over other renewable energy generating technologies like wind and solar. For example, wave energy production can be predicted 84 hours into the future, which will help utilities with load balancing [2]. Wave power also has less diurnal variations, so it can be available to provide base load at night unlike solar energy [3].

Despite all of these potential benefits, at this point in time wave energy technology is much less mature than wind or solar, resulting in a much higher levelized cost of electricity (LCOE) for wave energy compared to traditional sources of electricity. For wave energy to become a cost competitive source of electricity, its LCOE must be reduced to compete with other energy sources. LCOE can be reduced in two main ways; the cost of wave energy converter (WEC) can be reduced without impacting the power production, or WECs can be designed to produce more power without significantly impacting the cost of the device. In reality, both of these factors need to be addressed to continue to reduce the LCOE.

One current area of research to increase the amount of power produced by a WEC is to actively control it in such a way that average power output can be increased. The power take off (PTO) system can be configured to vary the amount of force exerted on the WEC to maximize power output. This has been an active area of research, with control algorithms such as model predictive control, dynamic programming, and other methods being proposed (e.g. [4, 5, 6]). However, all of these control strategies require some knowledge of the incident waves to determine what control actions will maximize power output. And most authors simply assume that these predictions will be possible, or propose solutions that make unrealistically optimistic assumptions.

This work presents a method that uses measurements of the motion of the WEC to estimate what the present excitation force on the WEC is. These force estimates

are then used to train an adaptive, autoregressive, prediction model to predict future excitation forces. This provides a method that uses the WEC itself as a measurement and prediction device, requiring only software and motions sensors, yielding a low cost solution. The method is tested in simulations on a generic point absorber WEC, and results are presented for a variety of estimators and predictors. While a point absorber model is used to test the model, the general technique could be applied to any WEC design that has approximate equations of motion developed.

The information flow through the different sections of the thesis is as follows. First a time domain model of a generic WEC is developed. This model is simulated under a variety of varying wave conditions, using recorded water surface elevation as the input to the model. The output to this model is excitation force, positions, and velocities of the WEC. Artificial white noise is then added to the true positions and velocities of the simulation results to better approximate what outputs would be generated by real sensor systems. These artificially noisy measurements are then used as the input to an estimation force estimator. This estimator provides estimates of the excitation forces at the present time from the artificially noisy measurements. The accuracy of these estimates can then be compared to the true excitation force as calculated from the WEC model. The estimated forces are then input to the prediction model, which uses these values to predict future excitation forces for the next 20 seconds. This prediction is performed at each time step, and the prediction accuracy can be determined by comparing to the true excitation force values that are calculated in the WEC model. Note that the true excitation force values are known in the simulation, but would not be known or measured in real-time on a deployed WEC. This information flow is summarized in the flow chart shown in Figure 1.1.
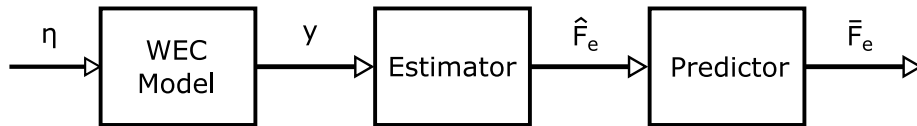
Figure 1.1: Flow chart showing the information flow of this thesis. η is the water surface elevation, y is the vector of noisy position and velocity measurements, $\hat{F}_e$ is the estimated excitation force, and $\bar{F}_e$ is the predicted excitation forces.

Chapter 2 provides a literature review on WEC control and short term prediction algorithms for WEC control applications. Next Chapter 3 presents the approach that was used to model the generic WEC used in this thesis. Then the different excitation force estimates are presented in Chapter 4, along with the estimation results applied to the generic WEC. Chapter 5 presents the methodology used for the predictors, followed by the prediction results. Finally the thesis concludes with a discussion of all the results and the methods in Chapter 6.

A note on terminology used in this work. The word *current* is used to refer to the present time throughout this work. Its usage should not be confused with ocean currents, another possible hydrodynamic force that is not considered in this work.

Chapter 2: Literature Review

There has been significant research on controlling wave energy converters (WECs) to increase power output. First Section 2.1.1 provides a brief overview of optimal control theory applied to the problem of maximizing absorbed power of a generic WEC. Then different control strategies that have been proposed are reviewed in Section 2.1.2. Finally a review of the current research on short term prediction schemes used for WEC control is given in Section 2.2.

2.1   WEC Control

2.1.1   Basic Theory

A WEC is harvesting power from a oscillating source, ocean waves. Regardless of the mechanism used to convert oscillations into usable power, to absorb the maximum available mechanical energy from the waves the WEC must generate a wave that interferes destructively with the incident wave, resulting in a still sea behind the device [7]. Another way of thinking about maximizing energy produced by a WEC is that it must *create* a wave that destructively interferes with the incident wave. This behavior is independent of the power take off (PTO), or energy conversion mechanism. The trajectory that generates a wave that destructively interferes with the incident wave will depend on the hydrodynamic properties of the specific WEC. If the WEC follows this optimal trajectory, the amount of kinetic energy that is transfered from the ocean waves to the wave energy converter body will be maximized.

In regular waves this can be achieved by forcing the WEC to oscillate at the same frequency as the waves, and at a specified phase shift from the water surface elevation. However, in an irregular wave environment, specifying the trajectory that optimizes power absorption becomes more difficult. For a device that is moving in heave, the optimal trajectory can be calculated in the frequency domain, then converted to the time domain to generate a desired trajectory to track [7]. This would require knowledge of the

future excitation force due to the non-causality of the excitation force impulse response function [7]. Other suboptimal control methods have been explored that reduce the required forward prediction horizon, but to apply wave-by-wave control most strategies require a prediction horizon of water surface elevation or wave excitation force. In the following subsection many of the recent proposed WEC control methods are reviewed.

2.1.2   Control Methods

The simplest way to control a WEC is to passively tune the PTO to maximize power output for a given sea state. The PTO is not changed on a wave by wave basis, but rather parameters such as the generator damping ratio are adjusted to match the mean wave period at the present time. While this method is simple to implement, it effectiveness at increasing power output is limited. Applying a wave by wave control algorithm allows the controlled WEC to come closer to realizing the optimal control.

The first widely proposed wave by wave control method for increasing the power output of WECs was proposed by Budal, and was termed latching control [8]. Latching control originated from the observation that for a single degree of freedom, the optimal velocity trajectory of the body is in phase with the wave excitation force. Latching control exerts a force to hold the buoy at its highest point until the excitation force waveform progresses forward enough to maintain the phase relationship with the devices velocity. At this point, the WEC is unlatched, allowing it to move again. This type of control presents many difficulties for implementation, including large forces on the latching mechanism, and difficulty determining when to unlatch the WEC. Much additional research has gone into improving latching control, however the high forces required to achieve latching in practice have caused researchers to begin exploring other control algorithms.

More modern control approaches have been proposed more recently. MPC has received a lot of research interest in WEC control. MPC calculates an optimal control over a finite horizon given a discrete system model, system constraints, and an estimation of future forces. The calculated control is implemented for a single time step, then the optimization is rerun with the new time horizon. This control approach is a good fit for control of WECs due to the fairly slow dynamics and ability to respect any potential system constraints. It does however require a prediction of future wave excitation forces

to implement.

MPC was applied to a single body heaving WEC by Brekken in [4]. This formulation involved tracking the velocity profile that corresponded with maximum power production. The current wave excitation force was estimated using a Kalman filter, and future forces were calculated using autoregressive least squares, however no details on the implementation of either of these algorithms was included in the paper. A nonlinear MPC approach was then investigated to account for nonlinear mooring forces by Richter et al. [9]. These authors showed that only marginal gains were realized when using a nonlinear MPC instead of linear MPC with a linearized mooring force for the test case. Another nonlinear MPC approach was used on a heaving point absorber by Tom and Yeung [10]. This controller was unique because no reactive power was permitted by the controller. Abraham and Kerrigan apply the results of optimal control theory to reduce the possible control input choices for a model predictive type controller [11]. They also study the sensitivity of power output to the prediction horizon, and show that a prediction horizon of 8 seconds is sufficient for their proposed control method.

Other more novel methods control methods to achieve optimal power production have been explored as well. Li et al. show the theoretical optimal control solution for a heaving WEC is bang-bang, which means that to maximize power the control force will abruptly switch between its minimum and maximum values [5]. They leverage this theoretical finding to significantly reduce the computational requirements of a dynamic programming algorithm. Their method doubles power output over an uncontrolled device. The algorithm requires 1-2 seconds of future excitation force predictions, and they assume that this would be available in their simulations. Schoen et al. use a combined robust fuzzy logic controller with a genetic algorithm to achieve good results with a short prediction horizon of 1 second [12]. Scruggs et al. use a modified linear Gaussian controller to develop a controller that does not require any excitation force predictions [13]. This causal control scheme is compared to the optimal control result, and is shown to increase power output over an uncontrolled device, but the increase is less that what is possible if excitation force predictions are used.

A table summarizing the prediction requirements and power increase of many predictive control schemes is shown in Table 2.1. Most controllers require prediction horizons between 1 and 10 seconds in idealized situations. We hypothesize that the size of the WEC, variations in local wave climates, and the reaction time of the PTO may slightly

Author(s) and Year	Prediction Horizon	Power Increase
Brekken 2011 [4]	20 s.	unknown*
Schoen et al. 2011 [12]	1 s.	50%
Li et al. 2011 [5]	1 s.	100%
Hals et al. 2011 [6]	2.2 s.	100%
Richter et al. 2013 [9]	3 s.	unknown*
Abraham and Kerrigan 2013 [11]	8 s.	100-400%
Scruggs et al. 2013 [13]	0 s.	unknown*
Tom and Yeung 2014 [10]	1.7-2.5 s.	25-50%

* uncontrolled case not presented in paper

Table 2.1: Summary of selected predictive WEC controllers. The prediction horizon used by each controller and the percent power increase over the uncontrolled case are listed.

increase the prediction requirements for many of these controllers. All the authors except Scruggs et al. acknowledge the need for some form of wave or excitation force prediction. The next section provides a review of the work that has been done in short term wave predictions for wave energy control applications.

2.2 Wave Prediction

Many of the proposed control strategies for WECs that were reviewed in the previous section have one thing in common; they require knowledge of future wave excitation forces. There has been some work done in making these predictions.

One approach is to measure the water surface elevation at one or more locations and then propagate those measurements forward using a wave dispersion model. The theory behind this technique, often referred to as deterministic sea wave predictions, has been studied extensively. It has the potential to make predictions over a large time horizon of multiple minutes [14]. However, the accuracy suffers greatly in multi-directional seas, and many wave measurement buoys are needed to make predictions at a single location, which will increase the cost of implementing deterministic sea wave predictions. Another challenge is adjusting the prediction model for the location of the WEC as it moves around in its watch circle.

While using measurement buoys to apply deterministic sea wave prediction has shown

to present many challenges, the theory behind the method has been applied using LIDAR to measure the upfield waves. A LIDAR device mounted on the WEC is used to scan the incident wave field in front of the floating object. The measured wave field is then propagated forward in space and time using a wave dispersion model to predict the future water surface elevation time series at the location of the WEC [15]. Using LIDAR instead of additional measurement buoys presents different challenges, including compensating the measurements for the movement of the WEC, the lower angle of the LIDAR system not being able to measure the water surface elevation behind the wave crests, and the additional costs associated with installing a LIDAR system on each WEC [16]. Sea trials testing this approach showed predictions with a low degree of accuracy are possible with current technology, but more research is required for higher accuracy predictions [17].

A third approach is to use the WEC itself to measure the water surface elevation or excitation force on the WEC, then use a mathematical model to predict the future elevations/forces from the recently observed elevations/forces. This class of methods has the benefit of not requiring a wave dispersion model, instead the elevations/forces are considered only at a single point. This allows a variety of time-series prediction methods to be used.

One approach that was proposed by Halliday et al. is to perform a discrete Fourier transform on the recently observed values to decompose the signal into its frequency components [18]. From the transform results, the magnitude, phase, and frequency of each component can be used to reconstruct the signal and propagate it forward in time to make predictions. Halliday et al. showed that this frequency domain prediction approach does not yield reliably accurate prediction accuracies when propagating forward in time only [18]. Real ocean waves have time varying frequency components [19], so a prediction model needs to be able to account for these time-varying properties. The discrete Fourier transform assumes the frequency content of the signal is stationary, which is what likely causes the poor prediction performance when used to predict forward in time.

Other methods that have been studied have been primarily autoregressive methods, which assumes the future time series values can be predicted as a function of previous time series values. In two consecutive papers Fusco and Ringwood study a variety of prediction methods applied to recorded water surface elevation predictions filtered with different low-pass frequency cutoffs [20, 21]. They show that the more high frequency content that is filtered out from the time series data, the more accurate the

predictions become. Their research included a variety of models, including linear autoregression, neural networks, and static and dynamic cyclic models used in conjunction with a Kalman filter. They found that the linear autoregressive prediction model yielded the best results in both sea states tested. The work did not discuss how to effectively choose training data for the autoregressive models, or address how measurement and filtering of the water surface elevation would be performed in real-time.

Schoen et al. also applied a variety of autoregressive prediction models to the wave prediction problem [12]. The four models these authors tested were the linear autoregressive model, linear autoregressive model with moving average, a Kautz filter, and a combination Kautz/autoregression model. The performance of these models was then evaluated on water surface elevation reconstructed from a Pierson Moskowitz spectrum with artificial added noise. The performance of the Kautz model and the linear autoregressive model were shown to be similar for the tested sea state. Schoen et al. then use the prediction methods developed in conjunction with a robust fuzzy logic controller that is shown to significantly increase power output of the simple WEC in simulations.

In 2014, Boren et al. investigated using an artificial neural network to make water surface elevation predictions [22]. A variety of neural networks were trained and evaluated using recorded water surface elevation data. The water surface elevation data was not filtered or otherwise modified from the original recorded data. The results were compared to a linear autoregression model, with no significant performance difference shown between the two approaches.

The research done on predictions thus far has focused on water surface elevation, or filtered versions of water surface elevation. Furthermore, adaptive techniques that can change as the wave conditions change, have not been thoroughly studied. This motivates more research into using the measured motions of the WEC to estimate excitation forces, and using these estimations in an adaptive prediction algorithm. The work in this thesis does exactly that, and tests the proposed algorithms on a generic WEC in a wide range of sea states.

Chapter 3: WEC Modeling

Modeling the motions of a floating body subject to waves has been investigated for many years. Models are often developed in the frequency domain, because some of the coefficients in the equations of motion have frequency dependent terms. In 1962 Cummins presented a method to simulate motions in the time domain using convolution integrals to convert the frequency dependent coefficients into the time domain [23]. This thesis works exclusively with a time domain model of the WEC, as the time domain formulation is more useful for generalized control designs. Some modifications are made to the Cummins formula to incorporate mooring and reduce the computational complexity.

This chapter is laid out as follows. Section 3.1 presents the theory describing WEC modeling. This is followed by a presentation of results for the generic WEC that is modeled in this thesis, in Section 3.2.

3.1 Developing Equations of Motion

The wave forces that act on a moving body consist of the excitation force and the radiation force. The excitation force (F_e) is the total force that would be exerted on the body if it were held motionless while subject to waves. The radiation force (F_r) is the dissipative force on the body due to the creation of radiative waves. Other forces included are the buoyancy force (F_b), the force due to mooring lines (F_m), and any control force from the power take-off system, or power generation system (F_u).

If we assume small displacements relative to the incident wavelength, and linear wave theory, then the equations of motion for a WEC can be written as

$$M\ddot{s} = F_r + F_b + F_e + F_u + F_m, \tag{3.1}$$

where s is the vector of positions and rotations that define the WEC's current position and orientation, and M is the inertia matrix that contains the masses and rotational inertias of the WEC for the different modes of motion. Note that Eqn. 3.1 is a vector equation with an order equal to the number of degrees of freedom being simulated.

The excitation force is a summation of two forces, the Frode-Krylov force and the diffraction force. Each of these forces is composed of independent components that act on each degree of freedom of the system. The magnitude and phase response of the excitation force for different frequencies of incident waves can be calculated with a hydrodynamic software package such as ANSYS Aqwa [24]. In this work, ANSYS Aqwa was used, which output the phase and magnitude response as a function of frequency ω, represented as a complex function of frequency, $\mathbf{F_e}(\omega)$. The impulse response function of the ith component of the excitation force ($F_{e_i}^{\mathrm{IRF}}$) is then calculated by taking the inverse Fourier transform of the frequency response, shown in Eqn. 3.2. It is worth noting that the excitation force impulse response function is typically non-causal, implying that knowledge of future water surface elevation values is needed to calculate the excitation force at any time instant [7].

$$F_{e_i}^{\mathrm{IRF}}(t) = \frac{1}{2\pi} \int_{-\infty}^{\infty} \mathbf{F_{e_i}}(\omega) e^{i\omega t} d\omega \tag{3.2}$$

In the Cummins formulation, the time domain excitation force signal ($F_{e_i}(t)$) is determined by convolving the water surface elevation with the impulse response function of the excitation force, as shown in Eqn. 3.3, where $\eta(t)$ is the water surface elevation.

$$F_{e_i}(t) = F_{e_i}^{\mathrm{IRF}}(t) * \eta(t) = \int_{-\infty}^{\infty} F_{e_i}^{\mathrm{IRF}}(t - \tau)\eta(\tau)d\tau. \tag{3.3}$$

The calculated excitation force is then treated as an exogenous input to the WEC model, since it does not depend on the motion of the WEC.

The radiation force is the dissipative force due to the radiated waves created by the motion of the WEC. The radiation force can be simplified using the Kramers-Kronig relationship, yielding

$$F_r = F_r' - \mu(\infty)\ddot{s}, \tag{3.4}$$

where $\mu(\infty)$ is the added mass matrix of the WEC at infinite frequency, F_r is the radiation force, F_r' is the radiation force component associated with the velocity of the WEC, and $\dot{s}$ is the velocity vector of the WEC [7]. F_r' can then be calculated with the following

equation,

$$F_{r_i}(t) = \sum_{j=1}^{n} F'_{r_{ij}} = \sum_{j=1}^{n} \int_{-\infty}^{t} F_{r_{ij}}^{\text{IRF}}(t - \tau)\dot{s}_j(t)dt, \tag{3.5}$$

where n is the number of degrees of freedom in the system, $F_{r_{ij}}^{\text{IRF}}$ is the impulse response function linking the ith and j^{th} modes of motion, F_{r_i} is the radiation force component acting on the ith mode of motion. The radiation force impluse response function is calculated from the real valued radiation frequency response $\mathbf{R_{ij}}(\omega)$ using Eqn. 3.6,

$$F_{r_{ij}}^{\text{IRF}} = \frac{2}{\pi} \int_{0}^{\infty} \mathbf{R_{ij}}(\omega)cos(\omega t)d\omega. \tag{3.6}$$

It has been shown that $F_{r_{ij}}^{\text{IRF}} = F_{r_{ji}}^{\text{IRF}}$, so for example a WEC modeled under planar motion (3 DOF) would require evaluation of 6 convolution integrals to calculate the total radiation force.

Under the assumption of small motions of the WEC, the hydrostatic restoring force is a linear function of the WEC's displacement, given as

$$F_b(t) = -Ks, \tag{3.7}$$

where $F_b(t)$ is the hydrostatic restoring force, and s is the position vector of the WEC. The constant matrix K is a proportionality constant that depends on the WEC's geometry. This hydrostatic stiffness matrix represents the change in submerged volume due to a change in position of the device, and was calculated in ANSYS Aqwa.

The PTO forces and mooring forces are included in this section as generic forces for completeness. The functional form of these forces will vary greatly depending on control system design and mooring design, and may be linear or nonlinear forces.

After applying all of these simplifications, the equations of motion of the WEC can be written as

$$(M + \mu)\ddot{s} - F'_r(\dot{s}) + Ks = F_e(\eta) + F_u + F_m. \tag{3.8}$$

The time dependency notation for each term is dropped in this equation, but the dependence of the radiation force on the velocity and the excitation force on the water surface elevation is written explicitly.

3.1.1   Radiation Force State Space Approximation

Calculating the radiation force using the convolution integrals in Eqn. 3.5 is computationally expensive. Additionally, the convolution formulation is inconvenient for applying many control design methods. An alternative is to develop a single input, single output, reduced order state space model for each entry in the radiation impedance matrix F_r'. A state space representation of the radiation force also makes applying many control algorithms to the WEC more straightforward. This approach to modeling the radiation force for a WEC was originally proposed by Yu and Falnes in 1995 [25]. Then in 2005 Kristiansen et al. presented a more streamlined approach that leverages modern state space realization and model reduction techniques [26]. This modern approach is what is presented and applied in this thesis.

First a higher order state space realization is calculated from the radiation impedance impulse response function. This realization is calculated using the algorithm outlined by Kung [27], and implemented using the MATLAB function `imp2ss` in the Robust Control Toolbox. This algorithm builds the Hankel matrix from the measured impulse response, then constructs a balanced discrete state space realization from the Hankel matrix. The discrete model is then converted to a continuous time model using a Tustin transformation. This algorithm is applied to each radiation impulse response function independently, yielding a separate state space realization for each entry in the radiation impedance matrix.

The resulting reduced state space model for the (i, j) component of the radiation force is given by

$$
\begin{aligned}
\dot{\zeta}_{ij} &= A_{r_{ij}}\zeta_{ij} + B_{r_{ij}}\dot{s}_j, \\
F_{r_{ij}}' &= C_{r_{ij}}\zeta_{ij} + D_{r_{ij}}\dot{s}_j,
\end{aligned}
\tag{3.9}
$$

where $\zeta_{ij} \in \mathbb{R}^{m_{ij}}$, where m is the number of states in the reduced order model. This state space model maps the input velocity $\dot{s}_j$ component to the radiation force component $(F_{r_{ij}}')$ approximation for each radiation force component depending on the complexity of the dynamics, as was done in [26].

Each of these state space models can be combined into one larger model that maps the velocity vector to the radiation force vector F_r'. This process will be shown for three

degrees of freedom ($n = 3$), but it can be expanded to any number of degrees of freedom from 1 to 6. The three degrees of freedom that will be considered are for planar motion. Each degree of freedom is described in Table 3.1. For three degrees of freedom, there are six unique radiation force components. One for each mode of motion, and another cross-component for interaction effects between each mode.

Name	Index	Description	Variable
surge	1	horizontal	x
heave	2	vertical	z
pitch	3	rotational	θ

Table 3.1: The description of the three degrees of freedom considered for the radiation approximation problem.

The combined reduced order state space model for the radiation force vector is

$$\dot{\zeta} = \underbrace{\begin{bmatrix} A_{r_{11}} & 0 & 0 & 0 & 0 & 0 \\ 0 & A_{r_{22}} & 0 & 0 & 0 & 0 \\ 0 & 0 & A_{r_{33}} & 0 & 0 & 0 \\ 0 & 0 & 0 & A_{r_{12}} & 0 & 0 \\ 0 & 0 & 0 & 0 & A_{r_{13}} & 0 \\ 0 & 0 & 0 & 0 & 0 & A_{r_{23}} \end{bmatrix}}_{A_R} \zeta + \underbrace{\begin{bmatrix} B_{r_{11}} & 0 & 0 \\ 0 & B_{r_{22}} & 0 \\ 0 & 0 & B_{r_{33}} \\ B_{r_{12}} & 0 & 0 \\ B_{r_{13}} & 0 & 0 \\ 0 & B_{r_{23}} & 0 \end{bmatrix}}_{B_R} \dot{s},$$

$$F'_r = \underbrace{\begin{bmatrix} C_{r_{11}} & 0 & 0 & C_{r_{12}} & C_{r_{13}} & 0 \\ 0 & C_{r_{22}} & 0 & C_{r_{12}} & 0 & C_{r_{23}} \\ 0 & 0 & C_{r_{33}} & 0 & C_{r_{13}} & C_{r_{23}} \end{bmatrix}}_{C_R} \zeta$$

$$+ \underbrace{\begin{bmatrix} D_{r_{11}} + D_{r_{12}} + D_{r_{13}} & 0 & 0 \\ D_{r_{12}} + D_{r_{13}} & D_{r_{22}} & 0 \\ D_{r_{13}} & D_{r_{23}} & D_{r_{33}} \end{bmatrix}}_{D_R} \dot{s}, \quad (3.10)$$

where $\zeta \in \mathbb{R}^{6m}$ is the concatenated state vector for calculating all the radiation force

terms, and $F'_r \in \mathbb{R}^3$. The same process that was used to construct this state space model for three degrees of freedom could be applied to develop a similar system for any number of degrees of freedom between 1 and 6. This process could also be expanded to apply to problems with multiple interacting floating bodies.

3.1.2   Full State Space Model

The state space model used to calculate the radiation force (Eqn. 3.10) can be combined with Eqn. 3.8 to create a state space model to simulate the motion of a WEC in multiple degrees of freedom. The excitation force, PTO force, and mooring forces are treated as exogenous inputs to the system.

Defining $J = (M + \mu)$ for notational simplicity, the system's state equation becomes

$$\dot{\xi} = \begin{bmatrix} -J^{-1}D_R & -J^{-1}K & -J^{-1}C_R \\ I & 0 & 0 \\ B_R & 0 & A_R \end{bmatrix} \xi + \begin{bmatrix} -J^{-1} & -J^{-1} \\ 0 & 0 \end{bmatrix} \begin{bmatrix} F_u \\ F_m \end{bmatrix} + \begin{bmatrix} -J^{-1} \\ 0 \end{bmatrix} F_e, \quad (3.11)$$

where $\xi = \begin{bmatrix} \dot{s}^T & s^T & \zeta^T \end{bmatrix}^T$ is the state vector and I is an appropriately sized identity matrix. All zeros also represent appropriately sized zero matrices. The excitation force is separated from the other inputs to indicate that it is an external disturbance that cannot be controlled. For a three degree of freedom system $\xi \in \mathbb{R}^{6(m+1)}$, where m is the order used for the reduced order radiation state space models. For the remainder of this thesis, Eqn. 3.11 is used for all simulations of the WEC model.

The output equation, Eqn. 3.12, assumes that all the displacements and velocities are measurable. This would be possible by using a sensor suite containing accelerometers, gyroscopes, and GPS. The output equation is given by

$$y = \begin{bmatrix} I & 0 \\ 0 & 0 \end{bmatrix} \xi + \nu, \quad (3.12)$$

where $I \in \mathbb{R}^{6 \times 6}$, all zeros are appropriately sized zero matrices, y is the vector of measurements, and ν is a vector of uncorrelated Gaussian white noise signals representing the noise from the sensor measurements. The implications of noisy measurements will be discussed in the following section.

Parameter	Variable	Value	Units
Dry Mass of Float	m_1	$67,773$	kg
Dry Mass of Spar	m_2	$14,227$	kg
Water Depth	h	50	m
Vertical Center of Gravity (w.r.t mean water line)	n/a	0.42	m
Generator Damping Raio	b_{gen}	1.0×10^5	$\frac{N-s}{m}$

Table 3.2: A list of the numeric values of parameters used for the generic WEC.

3.2   Numerical Results for a Specific WEC

The generic WEC used in this thesis is modeled after the L10 device that was built and tested by Oregon State University and Columbia Power Technologies [28]. A sketch of the model used in this thesis is shown in Figure 3.1, and the numeric values of some parameters are listed in Table 3.2. The dimensions were scaled up somewhat to be closer in size to many commercial WEC designs. This design was chosen as it is a fairly simple design that can be used to evaluate the feasibility of estimation and prediction schemes presented.

The design incorporates a cylindrical spar that is moored with a taut mooring line, and an outer float that can move vertically with respect to the spar. The mooring line is held taut by excess buoyancy in the spar, without the mooring line the still water line would be further down the spar. The PTO is a linear direct drive generator, with power being generated from the relative motion between float and spar. However, we will assume that the spar does not move in the heave direction, due to its small cross sectional area and the taught mooring.

Planar motion of the WEC is assumed, so the degrees of freedom are in heave, surge, and pitch. For simulation purposes, it is also assumed that the entire device moves together in surge and pitch, while only the float moves in heave. Interaction effects between the two bodies are neglected, as analysis results from ANSYS Aqwa shows them to be negligible. Also validating this assumption, the radiation and added mass frequency response data shows that the interaction terms between heave and surge, and heave and pitch, are effectively zero. This means the heave motion is effectively decoupled from the surge and pitch of the device.
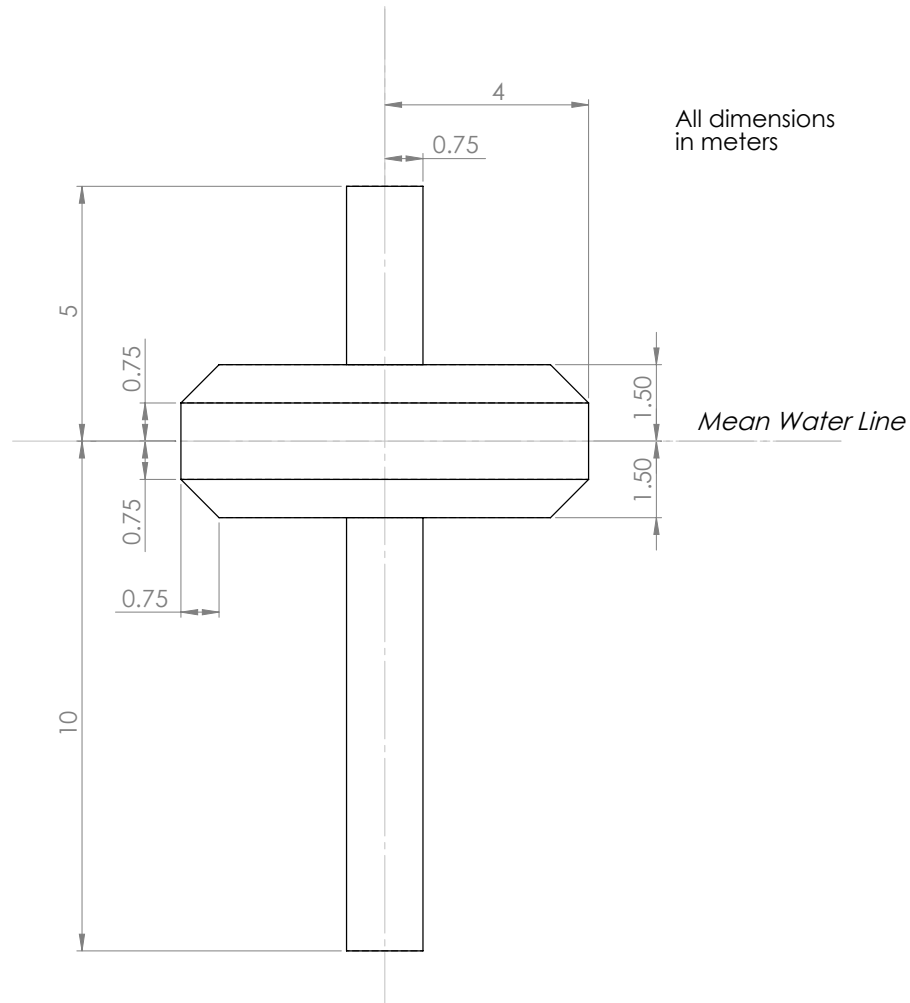
Figure 3.1: A sketch of the generic WEC that is modeled. Note that the geometry is symmetric about its vertical axis.

3.2.1 Frequency Response Data

The frequency response data for the excitation force, radiation damping, and added mass were all calculated in ANSYS Aqwa, over a frequency range of 0.02-1.0 Hz. Note that 1.0 Hz was used as the upper end cutoff as the water surface elevation data that is used

for simulations was recorded at 2.0 Hz. This makes 1.0 Hz the Nyquist cutoff frequency of the input signal which makes 1.0 Hz a good choice for a cutoff frequency for ANSYS Aqwa frequency response results. The data is shown in Figures 3.2 and 3.3.

The frequency response of the heave excitation force exhibits a different character than the surge and pitch components. As frequency approaches zero, the surge and pitch excitation force components approach zero, while in heave the force component approaches a non-zero value.

Figure 3.2: Plot of the excitation force frequency response. The first subplot shows the magnitude response ($|\mathbf{F_e}(\omega)|$), while the second subplot show the phase shift ($\angle\,\mathbf{F_e}(\omega)$).

Figure 3.3: Radiation force frequency response. The radiation force terms ($\mathbf{R}(\omega)$) are shown in the first subplot and the added mass coefficients ($\mu\omega$) are shown in the second plot.
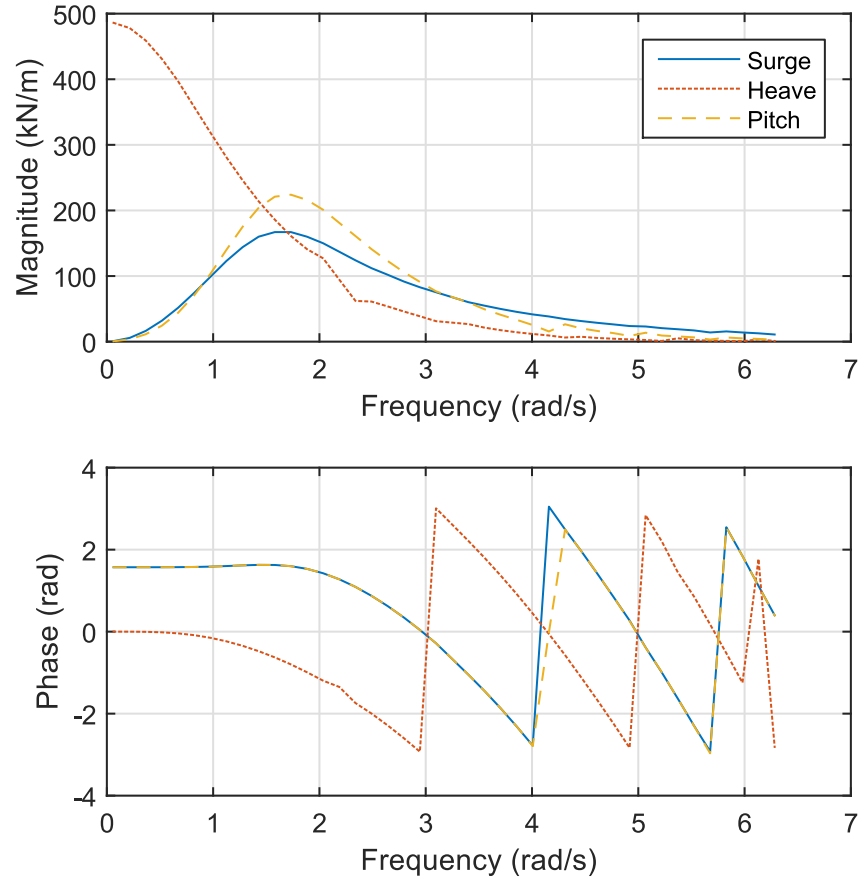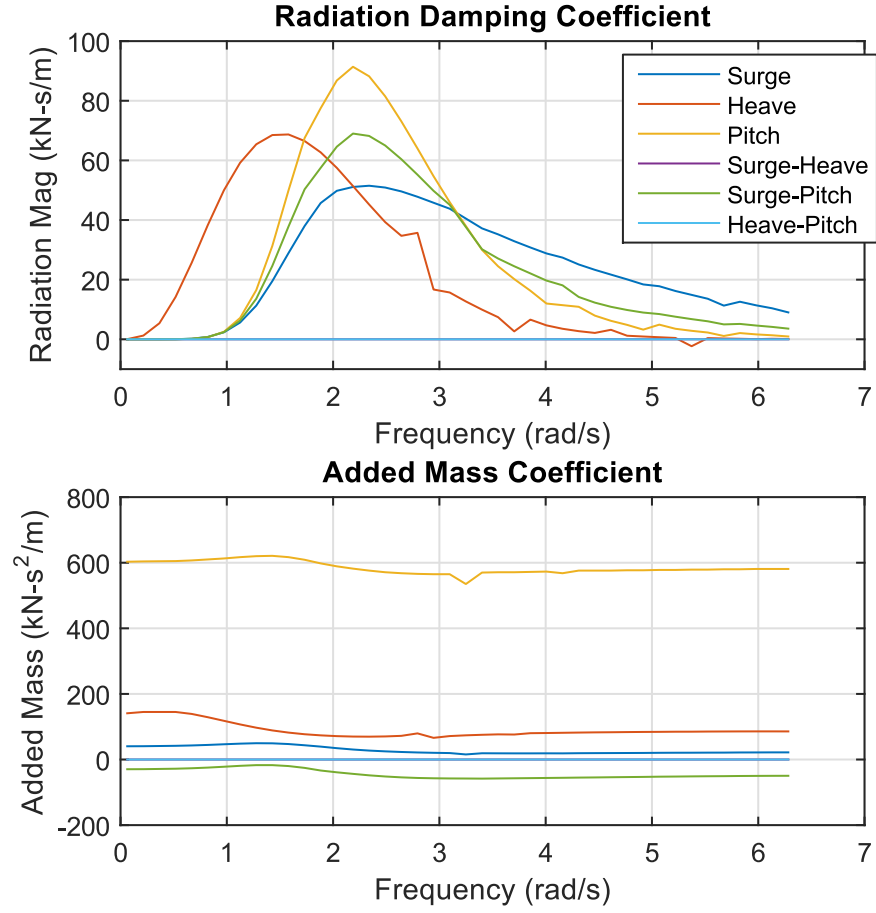
3.2.2   Impulse Response Functions

The excitation force impulse response functions are calculated using Eqn. 3.2 from the frequency domain results. The resulting impulse response functions for the modeled WEC are shown in Figure 3.4. The time variable in the impulse response can be interpreted to mean time ago, with the value of the impulse response at that time indicating the effect the water surface elevation at time t ago from the present time has on the excitation force value at the present time. Note that for $t < 0$, the impulse response for all three force components is not always zero, which says the relationship between excitation force and water surface elevation is non-causal. This means that the near future water surface elevation values are needed to calculate the excitation force at the present time.

A plot showing the radiation impulse response functions calculated from the frequency response is shown in Figure 3.5. The impulse response functions of the low order state space approximations are also shown. The order of the state space radiation was selected be $m = 8$, and this was done by increasing m until the impulse responses visually appeared to agree closely. The plot shows good agreement between the full impulse response and the low order approximation for all radiation force components. Also worth noting is the surge-heave and the heave-pitch terms are five orders of magnitude smaller than the other force components, making them effectively zero.
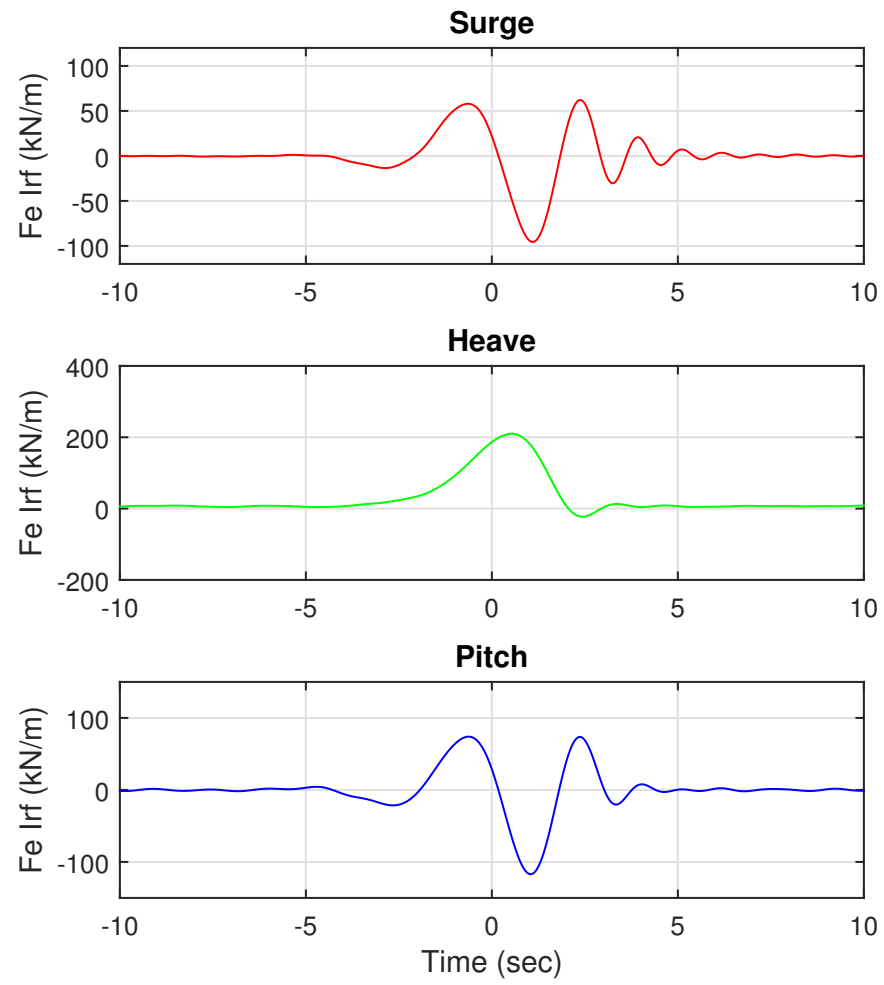
Figure 3.4: Plots of the excitation force impulse response functions.
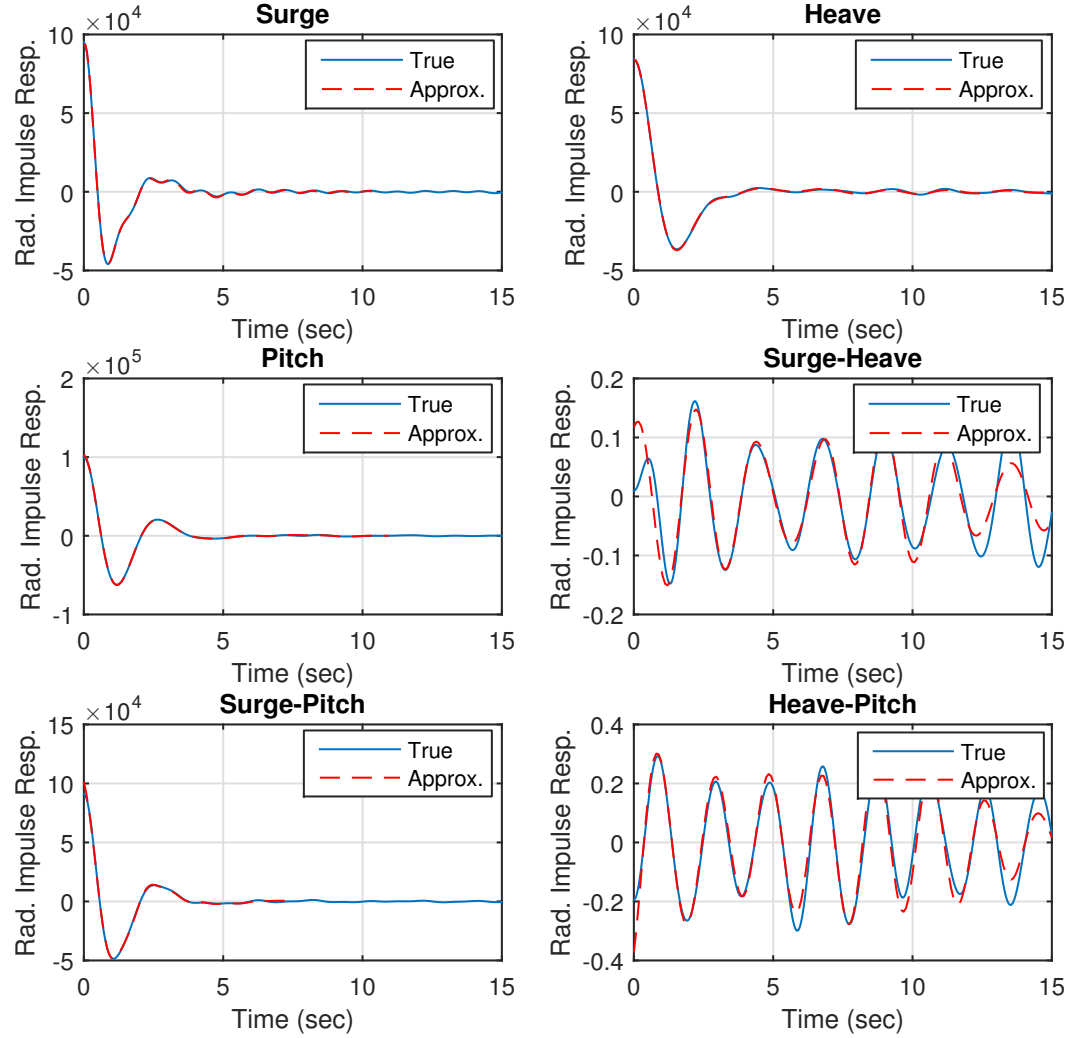
Figure 3.5: Radiation force impulse response functions. For each radiation term, bot the exact impulse response function and state space approximate impulse responses are shown. The order of approximation is $m = 8$.

3.2.3   Mooring and PTO Model

For a mooring configuration, a single vertical taut mooring line is assumed. This cable will be attached to the bottom of the spar, and pretensioned by the excess buoyancy in the spar. A free body diagram showing the mooring configuration and its associated forces in Figure 3.6.
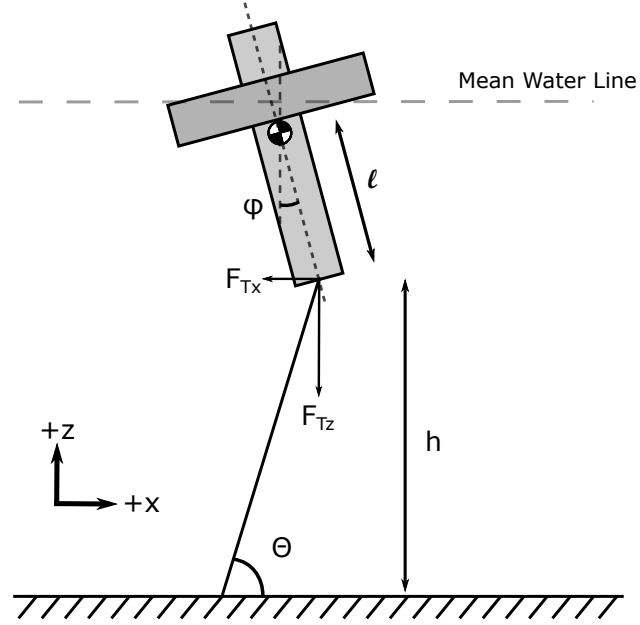
Figure 3.6: Free body diagram showing the mooring configuration and forces

The model assumes that the initial mooring cable tension is large enough to prevent significant displacements of the spar in heave. Therefore, the mooring force will only act on the surge and pitch modes of motion of the WEC. Also neglected are any hydrodynamic forces exerted on the cable, the cable tension is assumed to be the dominant force.

Given an initial cable tension T, and assuming the cable stiffness is set to keep the vertical component of the tension equal to the buoyancy of the spar, the total cable tension can be written as a function of cable angle θ as

$$F_T = \frac{T}{\sin \theta}. \tag{3.13}$$

Noting that $\tan\theta = \frac{h}{x + l\sin\varphi}$, where h is the vertical distance between the bottom of the WEC and the sea floor, and applying the small angle approximation $\sin\varphi \approx \varphi$, the surge component of the cable force can then be written as

$$F_{T_x} = -T\frac{\cos\theta}{\sin\theta} = -\frac{T}{h}x - \frac{Tl}{h}\varphi. \tag{3.14}$$

A similar process can be used to determine the moment the mooring cable exerts about the center of gravity of the spar, yielding

$$M_{T_{cg}} = -\frac{Tl}{h}x\cos\varphi - Tl\sin\varphi, \tag{3.15}$$

where φ is the pitch angle of the WEC and l is the distance between the bottom of the WEC and the center of gravity of the WEC. This can be linearized by taking the small angle approximation $\sin\varphi \approx \varphi, \cos\varphi \approx 1$, yielding

$$M_{T_{cg}} \approx -\frac{Tl}{h}x - Tl\varphi. \tag{3.16}$$

The total linearized mooring force can then be written in vector form as

$$F_m = \underbrace{\begin{bmatrix} -\frac{T}{h} & 0 & -\frac{Tl}{h} \\ 0 & 0 & 0 \\ -\frac{Tl}{h} & 0 & -Tl \end{bmatrix}}_{K_m} s. \tag{3.17}$$

The power takeoff force is calculated by using an idealized model for the linear generator. This model assumes the generator back force is linearly proportional to the relative heave velocity of the float with respect to the spar. Since we are assuming the spar's heave motion is negligible, the generator force is proportional to the heave velocity of the float. This can be written in matrix form as shown below in Eqn. 3.18

$$F_{\text{pto}} = \underbrace{\begin{bmatrix} 0 & 0 & 0 \\ 0 & b_{\text{gen}} & 0 \\ 0 & 0 & 0 \end{bmatrix}}_{B_{\text{gen}}} \dot{s}. \tag{3.18}$$

Equations 3.17 and 3.18 can then be added to the full state space model given by Eqn. 3.11. Since both the mooring and PTO forces are functions of state, they can be included in the A matrix of the state space model. This results in a final state equation model for the WEC as shown in Eqn. 3.19. The mooring and PTO forces do not change the output equation given in Eqn. 3.12.

$$
\begin{bmatrix} \ddot{s} \\ \dot{s} \\ \dot{\zeta} \end{bmatrix} = \begin{bmatrix} -J^{-1}(D_R + B_{\text{gen}}) & -J^{-1}(K + K_m) & -J^{-1}C_R \\ I & 0 & 0 \\ B_R & 0 & A_R \end{bmatrix} \begin{bmatrix} \dot{s} \\ s \\ \zeta \end{bmatrix} + \begin{matrix} -J^{-1} \\ 0 \end{matrix} \, F_e. \quad (3.19)
$$

This state space model is used to simulate the true motions of the WEC for the results presented throughout this thesis.

Chapter 4: Excitation Force Estimation

For a WEC that is operating in the open ocean, directly measuring the wave forces on the device would be very challenging. As mentioned in the introduction, many advanced control designs depend on knowledge of the wave excitation force. The hydrodynamic forces are caused by pressures distributed across the wetted surface area across the WEC. Measuring these in real time would require a large number of pressure sensors distributed across the surface of the WEC. Furthermore, these pressures represent the combination of all the hydrodynamic effects, including the excitation force, radiation force, and hydrostatic force. Discerning the portion of the total pressure due to each of these components in real time would be challenging, and likely be quite error prone.

Instead of trying to measure these forces directly, we propose estimating these forces by using more easily accessible measurements, and using the knowledge of the dynamics of the WEC to estimate the current excitation force. To make this estimation a Kalman filter is used. Kalman filters are a filter used to estimate the current state of a stochastic dynamic system from a set of measurements. We expand this classic estimation approach to estimate disturbances to the system, which in this case is the wave excitation force. The goal is to develop an estimator that provides accurate excitation force estimations over a wide variety of wave conditions.

This chapter is organized as follows. Section 4.1 describes how the Kalman filter formulation is adjusted to estimate system disturbances. Then Section 4.2 presents the simplified WEC model that is used in conjunction with the Kalman filter to estimate excitation forces. Numerical results are then presented in Section 4.3.

4.1   Kalman Filter for Disturbance Estimation

As mentioned previously, the Kalman filter is a common algorithm used to estimate the current state of a stochastic dynamic system. In fact, for a linear system with white Gaussian noise, the Kalman filter is the optimal state estimator [29]. This presentation of the theory of the Kalman filter is primarily from Simon [29].

Suppose we have a discrete state space model of the form

$$
\begin{aligned}
x_{k+1} &= Ax_k + Bu_k + \nu_k \\
y_k &= Cx_k + \omega_k \\
\nu_k &\sim N(0, Q) \\
\omega_k &\sim N(0, R)
\end{aligned}
\tag{4.1}
$$

where ν_k and ω_k represent the process and measurement noise respectively, with covariance matrices Q and R. The state vector at time step k is given as x_k, and y_k is the available output, or measurement, of the system. In this formulation, x_k, ν_k, and ω_k are unknown at step k. The goal of the estimation problem is to make the best estimate of x_k given y_k and the system model. This system model will be referred to as the Kalman predictor model.

Note that the system model can be a high fidelity model with many state variables, or a reduced order model. For a lower order model to be used, the state variables that are to be estimated must still explicit exist in the state vector. The errors introduced by the reduced order model can then be accounted for in the process noise vector ν_k. Assuming the process noise covariance is known completely, the tradeoff for using a reduced order model is reduced estimation accuracy for reduced computational complexity.

The Kalman filter is composed of two steps. Before the kth measurement becomes available the next state is predicted given the current state estimate using Eqn. 4.1. The state covariance P is also propagated forward using the system model. This step is shown in Eqn. 4.2 [29].

$$
\hat{x}_k^- = A\hat{x}_{k-1} + Bu_{k-1},
\tag{4.2}
$$
$$
P_k^- = AP_{k-1}A^T + Q,
\tag{4.3}
$$

where $\hat{x}_k^-$ is the a priori estimated state, $\hat{x}_{k-1}$ is the previous estimated state vector, and P_k^- is the a priori state covariance matrix. The term a priori is used to indicate before the measurement.

Once the measurement y_k is available, it is then used to "correct" the predicted a priori estimated state $\hat{x}_k^-$, yielding the a posteriori estimated state vector $\hat{x}_k$. This is done by calculating the Kalman gain K_k, then correcting the predicted estimated state

using Eqns. 4.4-4.6.

$$K_k = P_k^- C^T (C P_k^- C^T + R)^{-1}, \tag{4.4}$$

$$\hat{x} = \hat{x}_k^- + K_k(y_k - C\hat{x}_k^-), \tag{4.5}$$

$$P_k = (I - K_k C) P_k^-. \tag{4.6}$$

If the Kalman prediction model is nonlinear, it is still possible to use this general framework to make state estimates. This is done using the Extended Kalman filter (EKF), which as its name suggests extends the linear Kalman filter to nonlinear systems. First the next state is predicted using the full nonlinear Kalman prediction model instead of using Eqn. 4.2. Then the nonlinear system is linearized about the previously estimated state, $\hat{x}_{k-1}$. This linearized Kalman prediction model is then used with the rest of the algorithm, Eqns. 4.3-4.6.

The Kalman filter as presented above is the classical Kalman filter, used to estimate the state of the system. Suppose we add an unknown exogenous disturbance δ_k to our original Kalman prediction model The discrete state space model of this system is written as

$$\begin{aligned} x_{k+1} &= Ax_k + Bu_k + D\delta_k + \nu_k, \\ y_k &= Cx_k + \omega_k, \\ \nu_k &\sim N(0, Q), \\ \omega_k &\sim N(0, R). \end{aligned} \tag{4.7}$$

If the goal of the problem is to estimate the true value of δ_k as well as the true value of x_k, the Kalman filter will not provide estimates of the disturbance without modification. First, the Kalman prediction model is reformulated to include the unknown disturbance as additional states to the system, then the classic Kalman filter can be applied to estimate the disturbance δ_k.

To approach this disturbance estimation problem, first a simplified state space model

of the disturbance is created. This assumed model should be in the form

$$x_{d_{k+1}} = A_d x_{d_k} + \nu_{d_k},$$
$$\tilde{\delta}_k = C_{d_k} x_{d_k},$$
$$\nu_{d_k} \sim N(0, Q_d) \tag{4.8}$$

where the subscript d indicates disturbance model, $\tilde{\delta}_k$ is the modeled disturbance, and $\tilde{x}_{d_k}$ is the state vector of the disturbance model.

This disturbance model is then augmented to the original model given in Eqn. 4.7 to eliminate the disturbance term in the state update equation. Performing this substitution yields

$$\tilde{x}_{k+1} = \begin{bmatrix} A & DC_d \\ 0 & A_d \end{bmatrix} \tilde{x}_k + \begin{bmatrix} B \\ 0 \end{bmatrix} u_k + \tilde{\nu}_k,$$
$$y_k = \begin{bmatrix} C & 0 \end{bmatrix} \tilde{x}_k + \omega_k,$$
$$\tilde{\nu}_k \sim N \left(0, \begin{bmatrix} Q & 0 \\ 0 & Q_d \end{bmatrix} \right),$$
$$\omega_k \sim N(0, R), \tag{4.9}$$

where $\tilde{x} = [\ x^T\ x_d^T\ ]^T$ is the augmented state vector, $\tilde{\nu} = [\ \nu^T\ \nu_d^T\ ]^T$, and all zeros are appropriately sized vectors or matrices. The system model given in Eqn. 4.9 is then in the form of Eqn. 4.1, so the standard Kalman filter algorithm can be implemented to calculate the estimated augmented state vector $\hat{\tilde{x}}_k$. The estimated disturbances $\hat{\delta}_k$ can then be calculated from the estimated augmented state vector $\hat{\tilde{x}}_k$ by

$$\hat{\delta}_k = \begin{bmatrix} 0 & C_d \end{bmatrix} \hat{\tilde{x}}_k. \tag{4.10}$$

This is unnecessary if the estimated disturbances are contained in $\hat{\tilde{x}}_k$, in which case the estimated disturbances are simply extracted from the estimated augmented state vector $\hat{\tilde{x}}_k$.

This approach to estimating the disturbance of a dynamic system makes a few assumptions about the nature of the disturbance. The first is that an adequate state space model of the disturbance can be developed. The error of this model is captured in the

noise term ν_d. If this error is correlated, non-Gaussian, or non-zero mean, the Kalman filter is no longer the most optimal state estimation filter, although it can still be used to make estimates [29].

The second assumption is the covariance of the error associated with the disturbance model is known. This covariance matrix may be difficult obtain in practice, but the covariance matrix can be tuned to improve estimation performance. The tuning process used in this work is discussed in more detail in Section 4.3.

Using reduced models in the Kalman filter also adds complexity to the estimation problem. In state estimation, it is possible to use different system models of varying complexity with the Kalman filter to make state estimations [29]. These different models will have a tradeoff between estimation performance and computational complexity. This same tradeoff exists in the disturbance estimation problem. Different disturbance models could be used to make estimates, but some will be more accurate than others. By introducing reduced models to use with the Kalman filter, additional degrees of freedom are added to the estimator design process.

4.2   Simplified WEC Model for Kalman Filter

A framework for using a Kalman filter to estimate an unknown exogenous input was developed in the previous section. Now this section applies this disturbance estimation framework to estimation of wave excitation forces on a WEC. As mentioned in the previous section, it is possible to use different system models of varying complexity to perform the state estimation problem. As long as the state variables that are to be estimated are in the simplified state vector, then the simplified model can be used. Simplified models can be used to reduce the computational complexity of the filter, as the computational effort is related to the number of states in the prediction model.

There are two components of the WEC prediction model that can be reduced. First is the radiation force model, which was already modeled as a reduced order state space model in Chapter 3. The disturbance model can also be of varying complexity. Kalman prediction models of varying complexity are presented and evaluated for estimation of wave excitation forces.

4.2.1 Radiation Force Approximation

The simplest radiation force model is to assume the force is proportional to the WEC's velocity, i.e.,

$$\tilde{F}_r' = \bar{R}\dot{s}, \tag{4.11}$$

where $\dot{s}$ is the WEC velocity vector, $\tilde{F}_r'$ is the approximate radiation force, and $\bar{R}$ is an assumed matrix proportionality constant. This would reduce the WEC model from the state space model presented in Chapter 3 to

$$\begin{array}{c} \ddot{s} \\ \dot{s} \end{array} = \begin{array}{cc} -J^{-1}\bar{R} & -J^{-1}K \\ I & 0 \end{array} \begin{array}{c} \dot{s} \\ s \end{array} + \begin{array}{c} -J^{-1} \\ 0 \end{array} F_u + \begin{array}{c} -J^{-1} \\ 0 \end{array} F_e, \tag{4.12}$$

where J is the sum of inertia and added mass matrices, K is the sum of hydrostatic and mooring restoring force constants, F_u is the PTO force, and F_e is the excitation force. This formulation requires assuming a constant matrix $\bar{R}$, the choice of which will effect the prediction accuracy. This approach will be referred to as a zero order radiation force approximation ($m = 0$), as no additional state variables are used in the approximate model.

Another approach is to use the same radiation state space approximation methodology used in Section 3.1.1. A lower order model than was used for the original model can be used, or the full state space model developed in Chapter 3 can be used.

Both of these approaches are applied, and their prediction accuracies are compared. The best approach for an application will depend on how much computational resources are available for the estimation, and how well the process noise covariance Q can be determined.

4.2.2 Disturbance Model

Since the disturbance that is being estimated, the excitation force, is composed of a summation of sinusoidal signals, a natural choice for a disturbance model is to use a simple harmonic oscillator.

For a generalized number of independent harmonic oscillator disturbances, the state

space disturbance model can be written as

$$
\begin{aligned}
\begin{matrix} \dot{F}_e \\ \ddot{F}_e \end{matrix} &= \underbrace{\begin{matrix} 0 & I \\ -\bar{\Omega}^2 & 0 \end{matrix}}_{A_d} \begin{matrix} F_e \\ \dot{F}_e \end{matrix} \\[2em]
y &= \underbrace{\begin{matrix} I & 0 \end{matrix}}_{C_d} \begin{matrix} F_e \\ \dot{F}_e \end{matrix} \;,
\end{aligned}
\tag{4.13}
$$

where $\bar{\Omega}$ is a real diagonal matrix with entries corresponding to the assumed angular frequencies of the disturbance components, and F_e is the vector of disturbances, in this case excitation forces. This disturbance model is combined with the simplified WEC model given by Eqn. 4.12 to create a Kalman prediction model using Eqn. 4.9. Then this linear Kalman prediction model can be used to apply the Kalman filter to provide estimates of the excitation force, $\hat{F}_e$.

This disturbance model can be made adaptive by making the assumed frequencies in $\bar{\Omega}$ additional state variables. This makes the disturbance model nonlinear, which then requires use of the extended Kalman filter. It is assumed that the instantaneous frequencies change very slowly, so their derivatives are set to zero. Adding variance to these state variables allows them to slowly adapt over time. To write this disturbance model in a nonlinear state space form, first we will define the additional states as $\tilde{\omega} = [\, \tilde{\omega}_1 \, \tilde{\omega}_2 \, \tilde{\omega}_3 \,]^T$. For notational convenience, we then define

$$
\tilde{\Omega} = \begin{bmatrix} \tilde{\omega}_1 & 0 & 0 \\ 0 & \tilde{\omega}_2 & 0 \\ 0 & 0 & \tilde{\omega}_3 \end{bmatrix}.
\tag{4.14}
$$

Note that the $\tilde{}$ accent indicates variables that are now adaptive.

The nonlinear state space disturbance model, with adaptive frequencies, can then be

written as

$$
\begin{bmatrix} \dot{F}_e \\ \ddot{F}_e \\ \dot{\tilde{\omega}} \end{bmatrix} = \underbrace{\begin{bmatrix} 0 & I & 0 \\ -\tilde{\Omega} & 0 & 0 \\ 0 & 0 & 0 \end{bmatrix}}_{A_d} \begin{bmatrix} F_e \\ \dot{F}_e \\ \tilde{\omega} \end{bmatrix}
$$

$$
y = \underbrace{\begin{matrix} I & 0 & 0 \end{matrix}}_{C_d} \begin{bmatrix} F_e \\ \dot{F}_e \\ \tilde{\omega} \end{bmatrix}. \tag{4.15}
$$

This adaptive disturbance model can then be combined with the simplified WEC model given by Eqn. 4.12 to get a full Kalman prediction model, and then applied using the Extended Kalman Filter. This will yield estimated values of the excitation forces $\hat{F}_e$. Combinations of both of these disturbance models, and various reduced order radiation force approximations are all tested on the wave excitation force estimation problem.

4.3   Estimation Results

To test the performance of the estimators, first the WEC model developed in Chapter 3 is used to represent the true motion of the WEC. The input to the simulation is recorded water surface elevation time series data. The outputs of this model provide the true, or target values, for position, velocity, and excitation forces that can be used to evaluate estimation performance. The input to the estimators is simulated measurements from the full WEC simulation. These measurements are simulated by adding artificial white noise to the true position and velocities to simulate sensor outputs, sampled at 2 Hz. These noisy measurements then become the vector y_k in Eqn. 4.5 for use with the Kalman filter.

The WEC dynamic model presented in Chapter 3 is a continuous time model, but the Kalman filter is implemented in discrete time. All the Kalman prediction models presented in the previous section are developed in continuous time, so they must first be converted to discrete state space models. This is done in MATLAB using the function c2d, and using a first order hold on the input signal.

A few different estimators are tested, using different orders of radiation force approx-

imations, as well as different assumed frequencies for the excitation force models. Each of these estimators needed to be tuned to improve performance before they could be compared to each other.

Each estimator was initialized with a large initial prediction covariance matrix to minimize the effect of the initial state estimate. The sampling rate of the estimators were all set to 2 Hz, the same sampling rate as the recorded water surface elevation data. This is a sampling rate in the same order of magnitude that has been used by many proposed model predictive controllers, including [4].

4.3.1   Tuning the Estimators

The process noise covariance Q for each estimator is not fully known for any of the estimators, because the true value of many of the states is not known. For example, the states associated with the lower order radiation force state space approximation do not correspond directly to any state variables in the full order system. Instead, the covariance matrix can be tuned to improve the performance of the estimator. This tuning process was done automatically by optimizing the estimation accuracy of the estimated excitation forces using a non-gradient based optimization routine in MATLAB, `fminsearch`.

Using a formal optimization method to tune the estimators presents a few challenges. One is ensuring that the process noise covariance matrix Q remains both symmetric and positive definite, as required by the Kalman filter. This is done by assuming that Q is diagonal to ensure symmetry, an assumption that is often made when implementing Kalman filters. With a diagonal matrix, ensuring that each diagonal entry in Q will ensure positive definiteness. This issue is addressed by taking the absolute value of any entries in Q that the optimization algorithm set to negative values. The positive value was used when running the Kalman filter, while the value in the optimizer was left unchanged. This method proved to be more efficient than adding constraints to the optimization problem.

The other challenge in using an optimization algorithm for this process is formulating an objective function that represents how well the estimator is performing. The objective function should take on smaller values for better estimation, and should equally weigh the performance of the estimator on each excitation force component. After experimenting with many objective function formulations using both mean squared error and correlation

coefficients, the one that provided the best qualitative performance is given by

$$f(Q) = \sum_{i=1}^{n} \left(1 - R_i^2(Q)\right), \qquad (4.16)$$

where n is the number of degrees of freedom, and $R_i^2(Q)$ is the correlation coefficient of the estimated and true values of excitation force for the ith mode of motion. Note that the actual objective function is comprised of two steps. Before Eqn. 4.16 can be evaluated, the estimators are run for each of the test sea states. The correlation coefficients from these sea states are then used in Eqn. 4.16. A perfect estimator would be indicated by each correlation coefficient value being equal to one, which would result in an objective function value of zero. A correlation coefficient of zero indicates there is no relationship between estimated values and true values. Anything less than perfect would results in R_i^2 values less than one, which would increase the value of $F(Q)$. Note that in calculating the correlation coefficient, the slope of the best fit line is forced to a value of 1, and the intercept value is forced to zero, which would indicate an unbiased estimate. Correlation coefficient is used throughout the rest of this thesis to evaluate the accuracy of estimates and predictions, because it allows comparisons to data sets with different magnitudes.

A validation set was also used to ensure the model was not overfit to the training model. The training set consisted of four sea states representing the different conditions the WEC is expected to be subjected to. Each sea state data set consists of 40 minutes of water surface elevation data sampled at 2 Hz that was recorded using an AWACS acoustic monitoring device. The validation set consists of four additional sea states that were randomly selected from the 601 available sea states. During each iteration of the optimization algorithm, the performance of the validation set was also calculated following the same process as the training data. This yields two objective function values, one for the training data, and one for the validation data. A scatter plot of significant wave height and mean wave period for the training, validation, and all other available sea states is shown in Figure 4.1.

While using more time series data sets for training and validation may provide slightly better results for the overall test set, each additional data set that is used adds considerable computational effort to evaluating the objective functions. The training data is used by the optimizer, while the validation data is used to determine convergence, as
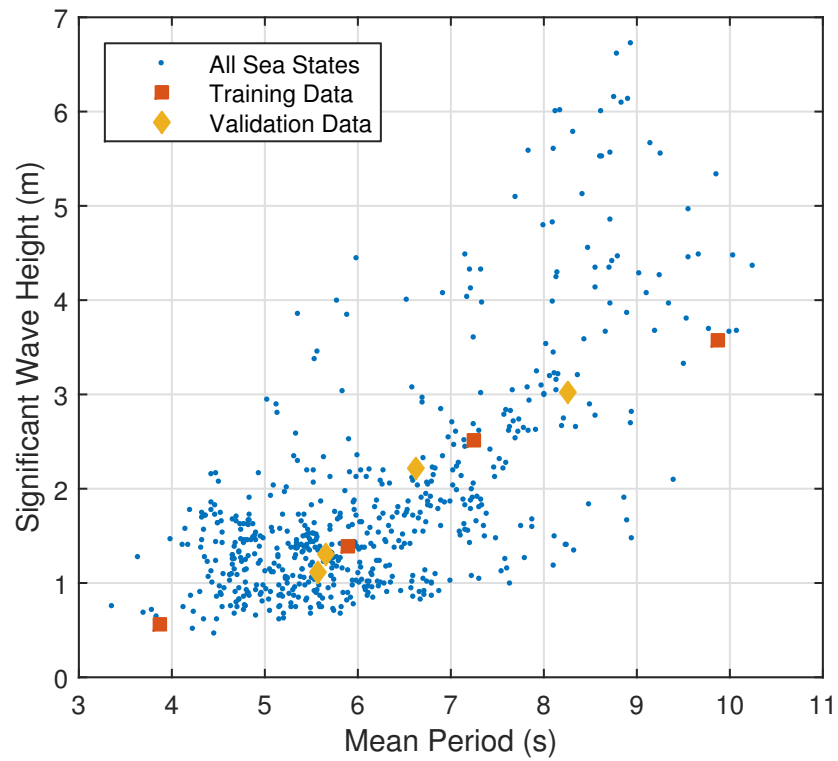
Figure 4.1: Significant wave height vs. mean period scatter plot of all available sea states. Shown are the 4 training data sets, the 4 validation data sets, and the remaining 593 states used to test the estimator.

discussed below.

There were two criteria that were used to determine convergence. One was a maximum number of function evaluations without improvement in the objective function. The other criteria prevented overfitting the estimators to the training data. If the performance of the training data continued to improve while the performance of the validation data becomes worse, the optimizer is stopped and the value of Q that resulted in the lowest value of the objective function for the validation data is returned as the optimizer. The optimizer is stopped when one of these two criteria are met.

Results from one of these optimization runs are shown in Figure 4.2. As can be seen, the training set objective function monotonically decreases as the optimizer continues to run. But after approximately 110 iterations, the objective function value for the validation data set begins to increase, causing the optimizer to eventually terminate, and select the optimal Q value as the one that resulted in the lowest objective function value from the validation data set.

Many different estimators were tuned, with different configurations. All combinations of a velocity proportional radiation approximation ($m = 0$), and 2nd and 4th order radiation state space approximations, along with four assumed values for $\tilde{\omega}$, and the adaptive disturbance frequency were all applied. The configuration of all the estimators that were evaluated is shown in Table 4.1.
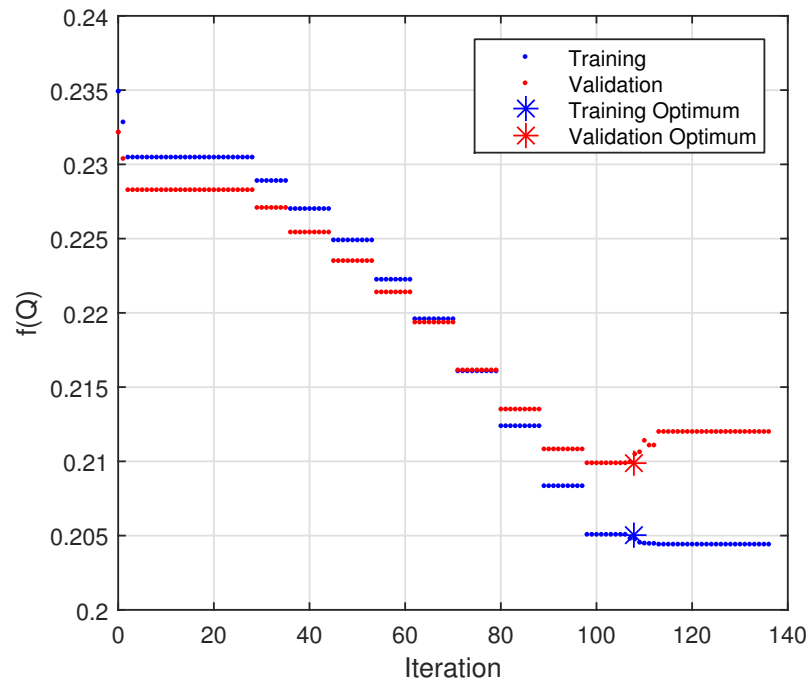
Figure 4.2: Estimation tuning optimization progress plot. For an example estimator tuning process the objective function value for the training and testing data set are shown at each iteration of of the optimization.

Index	Rad. S.S. Order	$\tilde{\omega}$ (Hz)	Num. States
1	0	$^1/_8$	12
2	0	$^1/_9$	12
3	0	$^1/_{10}$	12
4	0	$^1/_{11}$	12
5	0	Adaptive	15
6	2	$^1/_8$	24
7	2	$^1/_9$	24
8	2	$^1/_{10}$	24
9	2	$^1/_{11}$	24
10	2	Adaptive	27
11	4	$^1/_8$	36
12	4	$^1/_9$	36
13	4	$^1/_{10}$	36
14	4	$^1/_{11}$	36
15	4	Adaptive	39

Table 4.1: Configuration of the different estimators that were tested. The number of states in the model is also listed to illustrate computational complexity.

4.3.2   Estimation Performance

After each estimator was tuned using the procedure outlined above, its performance is evaluated over all 601 recorded water surface elevation time series shown in Figure 4.1. All 601 sea states are used to evaluate the performance because the goal of the disturbance estimator is to provide accurate estimations over the range of conditions a WEC would be subjected to. The correlation coefficient between the true excitation force and the estimated excitation force is calculated for each mode of motion, and each time series separately.

To compare the performance of the estimators, boxplots are created for each mode of motion that show the distribution of performance over the tested sea states. Figure 4.3 shows the heave estimation performance for each estimator. The blue box in the boxplot shows where the 25% and 75% values lie, the red line in the middle of the blue box indicates the median, and the black lines show the extent of the values that are not considered outliers. The red plus signs show outlier values, which is defined as being further than 1.5 times the interquartile range from the 25% or 75% value.

The mean regression coefficients for each estimator in heave is greater than 0.5, however, the estimators that have a fixed assumed frequency for the disturbance have a wide range of performance across different sea states. Using the adaptive frequency estimation technique greatly improves the worst case estimation performances in heave. For the estimators with fixed disturbance frequencies, a smaller assumed frequency value (longer period) results in a slight improvement in overall estimation performance. The lower order radiation approximations actually yield slightly better performances in heave when the disturbance frequency is fixed.

Next the performance of the estimators in the surge and pitch force components are shown in Figures 4.4 and 4.5. These two components are lumped together because their performance illustrates similar trends with respect to the different estimators. Estimation performance for surge and pitch shows much less variability, with the worst performance being much better than was seen with many of the estimators in heave. For both surge and pitch, using the velocity proportional radiation approximation ($m = 0$) results in much worse performance than when low order state space models are used. However, there is not a large performance difference between 2nd and 4th order radiation approximations in surge, and in pitch the estimators using the 4th order approximation
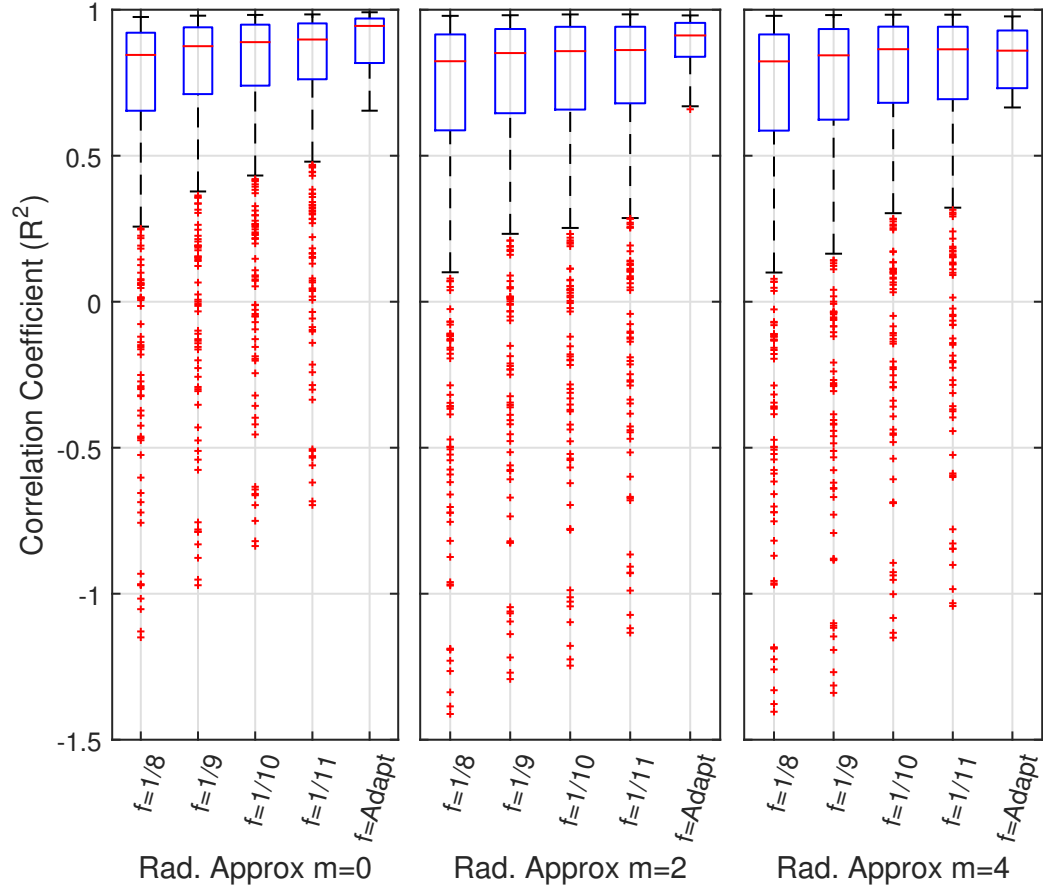
Figure 4.3: Boxplots showing the heave excitation force estimation accuracy evaluated using correlation coefficient for each of the 601 sea states tested. Each boxplot represents a different estimator, where f indicates the frequency in Hz of the disturbance model. Adaptive indicates an EKF estimator was used.

perform worse than using the 2nd order approximation.

In surge, faster assumed frequencies ($\bar{\omega}$) yield a slight improvement in estimation accuracy compared to slower frequencies. The adaptive frequency estimator performs similarly as the best fixed frequency estimator for each order of radiation approximation.

In pitch there is no consistent trend between estimation performance and assumed frequency, and the adaptive frequency approach appears to provide no additional performance improvements.

Since it is not possible to choose different estimator configurations for different modes of motion, one estimator has to be selected that performs the best over all three modes of motion. Since the adaptive frequency estimator provides a substantial performance improvement in heave, and using the second order radiation approximation provides a distinct improvement in surge and pitch, the 2nd order radiation approximation, adaptive frequency estimator is selected as the best estimator. This is the estimator that will be used to provide excitation force estimations to be used to generate future excitation force predictions in the next chapter.

The accuracy of the selected estimator is then plotted against the bulk statistics of each sea state it was tested with. Scatter plots of correlation coefficient vs. significant wave height and mean wave period are made for each excitation force component. These plots are shown in Figure 4.6.

Figure 4.6 shows a strong relationship between estimation performance and significant wave height for all the force components. When the significant wave height drops below approximately 2 meters, the estimation performance decreases significantly. A less prominent relationship between estimation accuracy and mean wave period is seen, with lower accuracies corresponding to shorter mean wave periods.

Figure 4.4: Boxplots showing the surge excitation force estimation accuracy evaluated using correlation coefficient for each of the 601 sea states tested. Each boxplot represents a different estimator, where f indicates the frequency in Hz of the disturbance model. Adaptive indicates an EKF estimator was used.
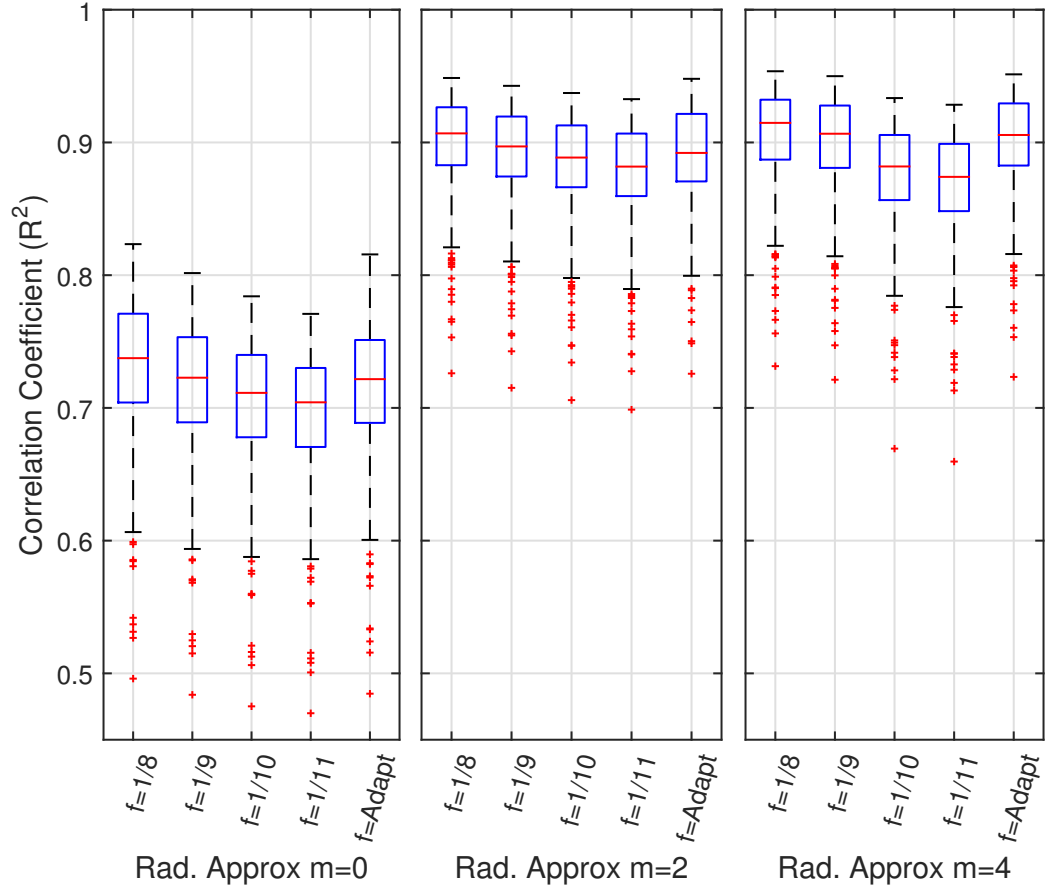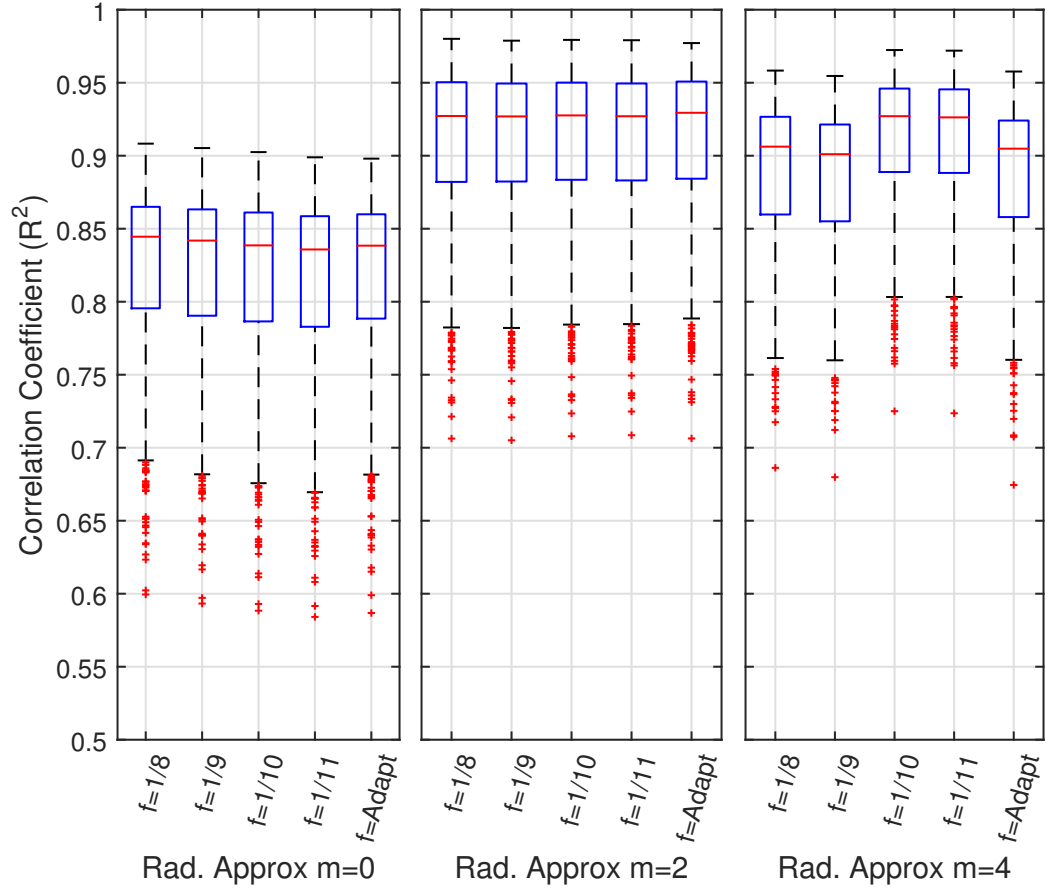
Figure 4.5: Boxplots showing the pitch excitation force estimation accuracy evaluated using correlation coefficient for each of the 601 sea states tested. Each boxplot represents a different estimator, where f indicates the frequency in Hz of the disturbance model. Adaptive indicates an EKF estimator was used.

Figure 4.6: Estimation performance vs. sea state parameters. For the selected estimator ($m = 2, \omega =$ Adapt), scatter plots of estimation performance against significant wave height on the left plots, and mean wave period on the right plots. The top row shows surge results, the middle row is heave results, and the bottom row is pitch results.

4.3.3   Discussion of Estimation Results

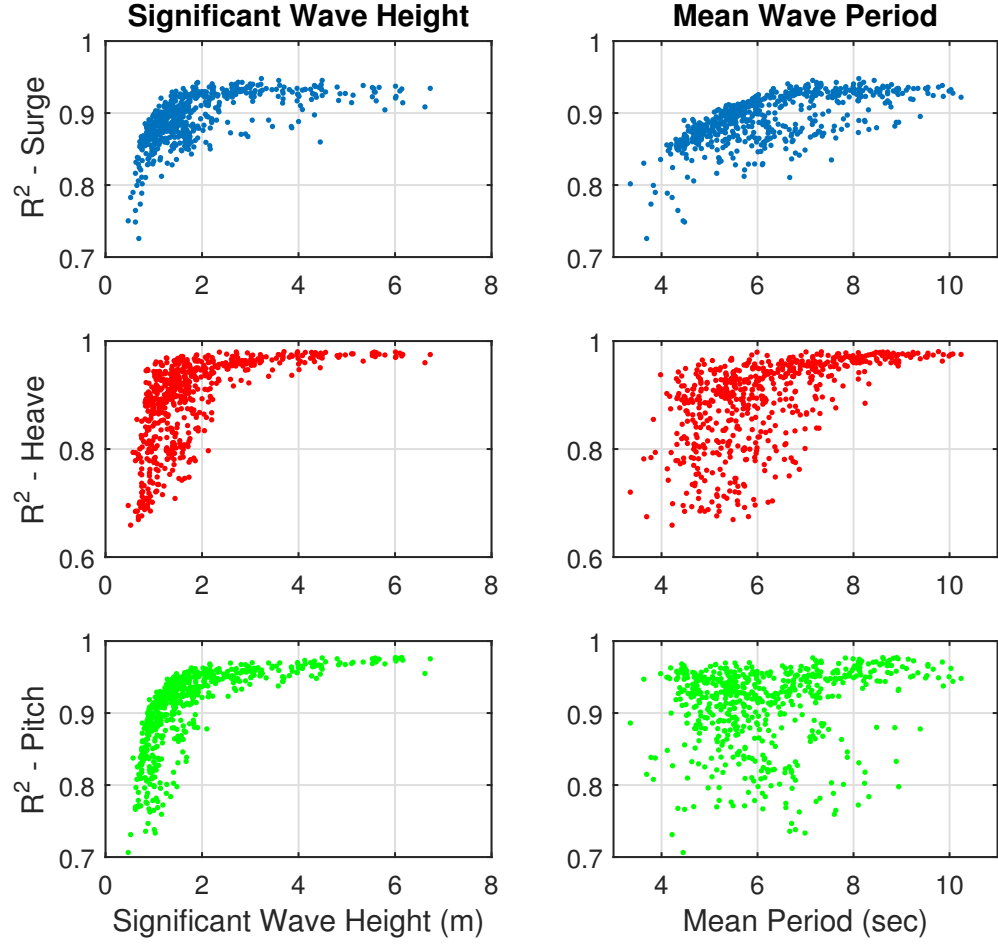The tuning of the disturbance estimator process noise covariance was posed as an optimization problem. This allowed the tuning to be performed automatically, and yielded better results than hand tuning the process noise covariance did, especially when the Kalman prediction model contained a large number of states. The method used was admittedly somewhat ad-hoc, and refining the automated tuning process is one possible area for future research.

There is a tradeoff in estimation between model accuracy and computational complexity. The more accurate the system model is, the more its predictions can be trusted, which results in more confidence in the state estimate. However, in this specific application, increasing the model accuracy is done by increasing the number of states used in the radiation force state space approximation. Since the true value of the states associated with these reduced order models are not known, the entries in the process noise covariance matrix corresponding to these states are set by optimizing the excitation force estimation performance. As the number of states in the prediction model grows, this optimization problem becomes more difficult. A smaller portion of the design space is then searched, and it is more likely that the optimization routine converged to a covariance matrix that results in a local minimum for estimation performance. This tradeoff between model accuracy and computational complexity likely explains why moving to a 4th order radiation force approximation did not result in a significant estimation performance improvement over the estimators utilizing a 2nd order radiation force approximation.

We also see a large difference in performance characteristics for the different estimators for the different force components. Surge and pitch seem have similar trends, while the trends for heave are significantly different. This is likely due to the nature of the frequency responses of the force components. From Figure 3.2, we can see that the going from water surface elevation to heave acts as a low-pass filter, attenuating high frequency components of the input signal. In surge and pitch, the relationship more closely resembles a bandpass filter, attenuating both high frequency and low frequency components of the signal. This may explain why the adaptive frequency disturbance model improves heave estimations much more than it does for surge and pitch. Presence of more energetic low frequency components of the water surface elevation will have a large effect on the heave excitation force signal, but much less so for surge and pitch.

This may also explain why lower fixed disturbance frequencies improved the estimation accuracy in heave, but decreased estimation accuracies in surge and pitch.

This same estimation approach can be applied to any other WEC design, as long as a system model of the device can be written in state space form. It would be possible to incorporate additional nonlinearities such as viscous damping by using the EKF. Estimation accuracy will depend on the accuracy of the model and the hydrodynamic properties of the WEC.

Chapter 5: Excitation Force Prediction

Now that a method of estimating present excitation forces at the current time step from readily available measurements has been presented, the next step is to use these estimated forces to predict future excitation forces. Many predictive control algorithms proposed for use with WECs require predictions of future excitation forces to yield significant performance gains. The goal of this chapter is to expand on the previous water surface elevation and excitation force research that was reviewed in Chapter 2. This is done by developing an adaptive version of the autoregressive least squares predictor that uses estimated excitation forces to predict future forces. The performance of the predictor is then quantified in a wide variety of sea states to illustrate the effect local wave climate has on prediction accuracy.

There are two approaches that can be taken to make predictions. One is to predict future values of water surface elevation, then use these predicted water surface elevations to calculate the excitation force. This requires a longer horizon of accurate predictions then if the excitation force is predicted directly, as some of the prediction horizon is lost due to the non-causality of the excitation force impulse response function [30]. This non-causality implies that future water surface elevations are required to calculate the current excitation force value. For example, if a proposed control algorithm requires 5 seconds of excitation force predictions, and the non-causality of the impulse response function is 5 seconds, then 10 seconds of accurate water surface elevation predictions are required, while only 5 seconds of predictions are required if the excitation force is predicted directly.

The approach taken in this thesis is to predict excitation forces directly. This way the forces can be estimated from the motion of the WEC without additional wave sensors upfield of the WEC.

The prediction approach taken in this thesis is driven by data; instead of relying on the underlying physics to develop a model, data is used to train a model to match previous recorded data. The resulting model structure is based less on physics and more on its ability to match the input-output pairs that were used to train the model.

There are many approaches to data driven modeling that vary in model complexity and capabilities, ranging from the simple autoregressive least-squares model to complex models such as artificial neural networks. As discussed in Chapter 2, many of these methods have been used to predict water surface elevations autoregressively. Two of these papers, Boen et al. and Fusco and Ringwood, both show that using an artificial neural network provides minimal gains over using an autoregressive least squares model [22, 21]. However, these proposed methods require training the prediction methods offline, and provide no method to allow the models to adapt to the changing wave climate that a real WEC would be subjected to.

This chapter presents a wave excitation force prediction method that addresses some of these gaps in the current literature. The autoregressive least-squares algorithm is modified to update recursively. The effect of using estimated excitation forces instead of actual estimation forces or water surface elevation as input to the prediction model is also explored. More precisely, the estimation results from the estimator developed in Chapter 4 are used as the input to the prediction model developed in this chapter. And finally, the input water surface elevation data that is used to generate the true excitation force signal is from recorded data, to ensure the non-stationary properties of real ocean waves is accounted for.

The chapter is organized as follows. Section 5.1 presents the autoregressive least squares model and the recursive version of this model. Then the results of the prediction model are presented in Section 5.2. The results section is broken into two subsections, with first subsection describing how the configuration parameters of the predictor were set, and the second subsection presenting numerical prediction results.

5.1   Prediction Model

This section will present the recursive, autoregressive least squares prediction model applied to a single time series. To apply to predicting all the components of excitation force, each component will be predicted using an independent prediction model.

An order n linear autoregressive prediction model is defined as

$$\bar{F}_e(k+1|k) = \sum_{i=0}^{n-1} \beta_i \hat{F}_e(k-i), \tag{5.1}$$

where $\hat{F}_e(k)$ is the excitation force value estimated with the Kalman filter at step k, $\bar{F}_e(k+1|k)$ is the predicted excitation force at $k+1$ given excitation force estimations up to step k, and $\beta \in \mathbb{R}^{n \times 1}$ is the vector of regression parameters.

Predictions multiple steps in the future are made by assuming the previous prediction is correct, and using the same coefficients to propagate the prediction forward as shown below,

$$\bar{F}_e(k+2|k) = [\bar{F}_e(k+1|k) \; \hat{F}_e(k) \; \cdots \; \hat{F}_e(k-n+2)]\beta. \tag{5.2}$$

This approach can be used to make predictions forward for an arbitrary number of forward steps. In the rest of this thesis, the term prediction horizon is used to indicate how far forward in the future a prediction is made.

In this model, the vector β defines the model, and the values of β must be determined from previous observations. If a set of p estimated force values are available, Eqn. 5.1 can be written in matrix form as

$$\underbrace{\begin{bmatrix} \bar{F}_e(n+1|n) \\ \bar{F}_e(n+2|n+1) \\ \vdots \\ \bar{F}_e(p|p-1) \end{bmatrix}}_{G} = \underbrace{\begin{bmatrix} \hat{F}_e(n) & \cdots & \hat{F}_e(1) \\ \hat{F}_e(n+1) & \cdots & \hat{F}_e(2) \\ \vdots & & \vdots \\ \hat{F}_e(p-1) & \cdots & \hat{F}_e(p-n) \end{bmatrix}}_{H} \beta. \tag{5.3}$$

As long as $p > n$, this results in a set of overdetermined linear equations. The regression parameters that minimize the sum of squared errors of this model can be calculated deterministically by solving the normal equations [31],

$$\beta = \left[H^T H\right]^{-1} H^T G. \tag{5.4}$$

This is the autoregressive least squares method used by most of the works discussed in Chapter 2. It presents many additional decisions when designing a predictor to be used on a WEC subjected to a variety of ocean conditions. These decisions include what data should be used to train the predictor, if different predictors should be used in different conditions, how many observations should be used to train the model, and how these different wave conditions would be defined. These issues arise because once β is determined using Eqn. 5.4, it cannot adapt to changing conditions.

To allow the prediction model to adapt to changing conditions, we keep the same model structure, autoregressive least squares, but use a recursive update algorithm to change the regression coefficients after each prediction is made. This is done by modifying the classic recursive least squares algorithm, presented in Ljung [31] and others, to apply to a predictor. It is modified to reflect the fact that at the current step k, the target output ($\bar{F}_e(k+1)$), is not known. It does not become available until the next time step, since it is value to is to occur in the future.

Defining x_k^* to be the vector of the previous n estimated excitation force values, or regressors vector, as

$$x_k^* = \begin{bmatrix} \hat{F}_e(k) & \hat{F}_e(k-1) & \cdots & \hat{F}_e(k-n+1) \end{bmatrix}, \tag{5.5}$$

and β to be the vector of regression coefficients,

$$\beta_k = [\beta_1 \; \beta_2 \; \cdots \; \beta_n]^T, \tag{5.6}$$

then the recursive least squares algorithm is given by [31]

$$\beta_k = \beta_{k-1} + \frac{P_{k-1}x_{k-1}^*}{\alpha + x_{k-1}^* P_{k-1} x_{k-1}^{*\top}} \left(\hat{F}_e(k) - x_{k-1}^* \beta_{k-1} \right), \tag{5.7a}$$

$$P_k = \frac{1}{\alpha} \left(P_{k-1} - \frac{P_{k-1}x_{k-1}^* x_{k-1}^{*T} P_{k-1}}{\alpha + x_{k-1}^* P_{k-1} x_{k-1}^{*T}} \right), \tag{5.7b}$$

$$\hat{F}_e(k+1|k) = x_k^* \beta_k, \tag{5.7c}$$

where P_k is approximately the covariance of the prediction, and α is a forgetting factor. Then Eqn. 5.2 can be applied to make predictions multiple steps into the future. The matrix P can be interpreted as indicating how much trust one has in the current estimate of the regression coefficient vector β. A larger 2-norm of P indicates less trust in the coefficients β. The forgetting factor can take on values between 0 and 1. A forgetting factor of 1 indicates that each measurement is weighted equally when updating the regression coefficients. This means that as time goes on, the incremental effect of the kth measurement diminishes, and β will converge to a steady state value. By setting α to a value less than one, previous measurements will be exponentially discounted by α^q,

where q is the number of steps in the past the measurement occurred. This allows β to slowly adapt as the underlying process changes [31].

One issue with including the forgetting factor in the recursive least squares algorithm is if the estimated parameters β do not vary enough over time, eventually the forgetting factor can cause the 2-norm of P to begin to grow. This can be remedied by monitoring for increases in the 2-norm of P, and if increases are detected P is reset to the initial value P_0. This will prevent the algorithm from diverging. In the work presented here, no divergence of P was observed so resetting of P was not implemented, although it is something that would need to be considered if implementing in real time.

Using a recursive autoregressive prediction model inherently allows the predictor to adapt to changing sea conditions. Instead of having to address how predictions will be made in different conditions by generating different models and switching between them, the design process is reduced to selecting the number of regressors to be used, and the forgetting factor value.

This algorithm is then applied independently to each component of the excitation force, yielding predictions for all excitation force components.

5.2   Prediction Results

Predictions were tested by using the estimated excitation force values generated from the extended Kalman filter as the input to the predictor. Prediction accuracy was then evaluated by comparing these predicted values to the true excitation force values that were generated from the WEC model. The predictor is initialized at each sea state by setting the initial covariance P to a diagonal matrix with large non-zero entries to reflect low initial confidence in the estimate of the regression coefficients. The initial regression coefficients used represent a persistant predictor, i.e. $\bar{F}_e(k+1) = \hat{F}_e(k)$. Another option that was not explored may be to perform regular least squares on a sample set of data to develop a better initial guess for β.

5.2.1   Determining Parameters

The number of regressors n and the forgetting factor α need to be set to apply the recursive prediction algorithm. The optimal values for n and α are determined using a

Parameter	Variable	Value
Num. Regressors	n	60
Forgetting Factor	α	0.999

Table 5.1: Configuration parameter values for prediction model.

two step process. First a constant value for the forgetting factor is set, and predictors with varying number of regressors are run on the same four sea states that were used to train the estimators (see Figure 4.1). The prediction performance over all four sea states is evaluated at three distinct prediction horizons. This generates a family of trade-off curves, one for each force component and prediction horizon combination, between prediction accuracy and model complexity. This curve is shown in Figure 5.1.

The first thing that is observed from the tradoff curves is for each force component and each prediction horizon, correlation coefficient does not monotonically increase with respect to the number of regressors. This is likely due to the fact that estimated values are the input to the predictor, but the prediction performance is being calculated by comparing to the true force values. This indicates that adding more regressors will not always result in an increase in performance, as a model that is too complex begins to overfit the noise that is present in the estimations.

The best performance for each mode of motion and at each prediction horizon occurs at at different number of regressors. If actually deploying this system, it would be possible to choose a different number of regressors for each force component. To simplify this work however, the number of regressors used for each mode of motion is the same. To get the best prediction performance across each of the modes of motion, and at all time horizons, the number of regressors that was chosen for this WEC is 60. For a specific WEC design, many factors may effect this choice, such as the wave climate it will be deployed in and its hydrodynamic properties.

Next the forgetting factor needs to be chosen. Simulations were run with a variety of forgetting factors ranging from 0.9 to 0.9999. A forgetting factor with a value closer to 1 will adapt more slowly, but also weight more previous recorded data in being used when determining the regression coefficients. For this WEC, in this wave climate, a forgetting factor of 0.999 provided the most favorable results over the four training sea states. The selected parameter values that are used for the predictor are summarized in Table 5.1.
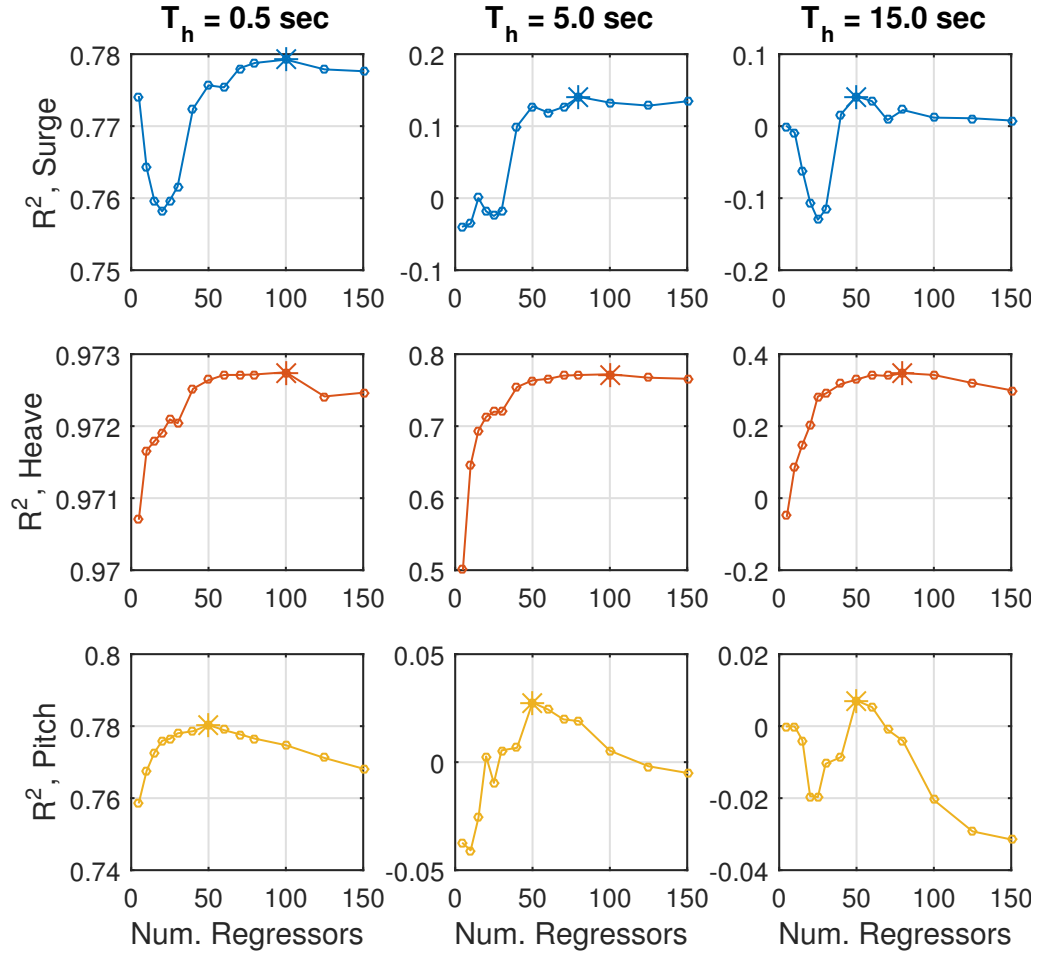
Figure 5.1: The family of prediction performance vs. number of regressors tradeoff curves. The top row of plots shows surge, the middle row shows heave, and the bottom row shows pitch. Each column of plots is associated with a different prediction horizon from 0.5 s. to 15.0 s. The maximum correlation coefficient for each tradeoff curve is indicated with a ∗.

5.2.2 Numerical Prediction Results

After setting the configuration of the predictor using the four training sea states, prediction results were generated for all 601 sea states. The predictor was reinitialized as discussed in the previous subsection at the beginning of each sea state.

The first result presented is an example time series output from the estimator and predictor. There are three subplots, showing three different snapshots in time spaced 2.5 seconds apart. The plot shows the true excitation force calculated using Eqn. 3.3, the estimated excitation force $\hat{F}_e$ for all time $t < 0$, and the predicted excitation force $\bar{F}_e$ for time $t \in [0.5, \ 20]$. Note that the time axis represents delta time from the current time, so $t = 0$ is the present time, positive values of t indicate future values, and negative values of t are past time points. This graphic, shown in Figure 5.2, is shown to illustrate the process of estimating excitation forces and predicting future forces. Since there are multiple predicted force values, the accuracy of the predictions at each prediction horizon can be calculated. This provides an indication of how accurate the predictions are at different intervals into the future.

To evaluate the performance of the predictor for a single sea state, the correlation coefficient at each discrete prediction horizon can be plotted on a scatter plot with prediction horizon on the x-axis, and correlation coefficient on the y-axis. A correlation coefficient of 1 indicates perfect prediction accuracy, and lower values indicate reduced accuracy. This displays how well the predictor does at different future time horizons. Combining these results for all the sea states that the predictor was tested on yields a distribution of correlation coefficients at each prediction horizon. This is displayed with a boxplot at each prediction horizon that shows the distribution of performance. The boxplots have the same configuration as before, with the box showing the 25th thru 75th percentile values, the whiskers showing all values within 1.5 times these percentile values, and outliers indicated with red plus signs. This plot is generated for each excitation force component, heave, surge and pitch. After presenting the results for all sea states as distributions, relationships between the prediction performance and different sea conditions are presented. The heave excitation force prediction performance is shown in Figure 5.3.

The heave force predictions have a wide distribution of accuracy over all the prediction horizons. For most sea states, relatively accurate predictions are maintained for

a prediction horizons from 0.5-6.0 seconds. For some sea states, accurate predictions extend much further into the future, while other sea states prediction accuracy drops very quickly to a correlation coefficient of zero.

Boxplots of the prediction performance for the surge and pitch force components are shown in Figures 5.4 and 5.5. At each prediction horizon, there spread of correlation coefficients is not as wide for surge and pitch as it is for heave. Prediction performance decreases rapidly with increasing prediction horizon, with good predictions only being made for a horizon of approximately 2.0 seconds into the future.

The prediction performance varies greatly between the different force components. Since the prediction method used for each force component is the same, there must be some external cause the differences in prediction performance. One possible explanation is that the prediction accuracy depends on the estimation accuracy. Another possible explanation is that the differences depend on the underlying physical processes that generate the excitation force signals.
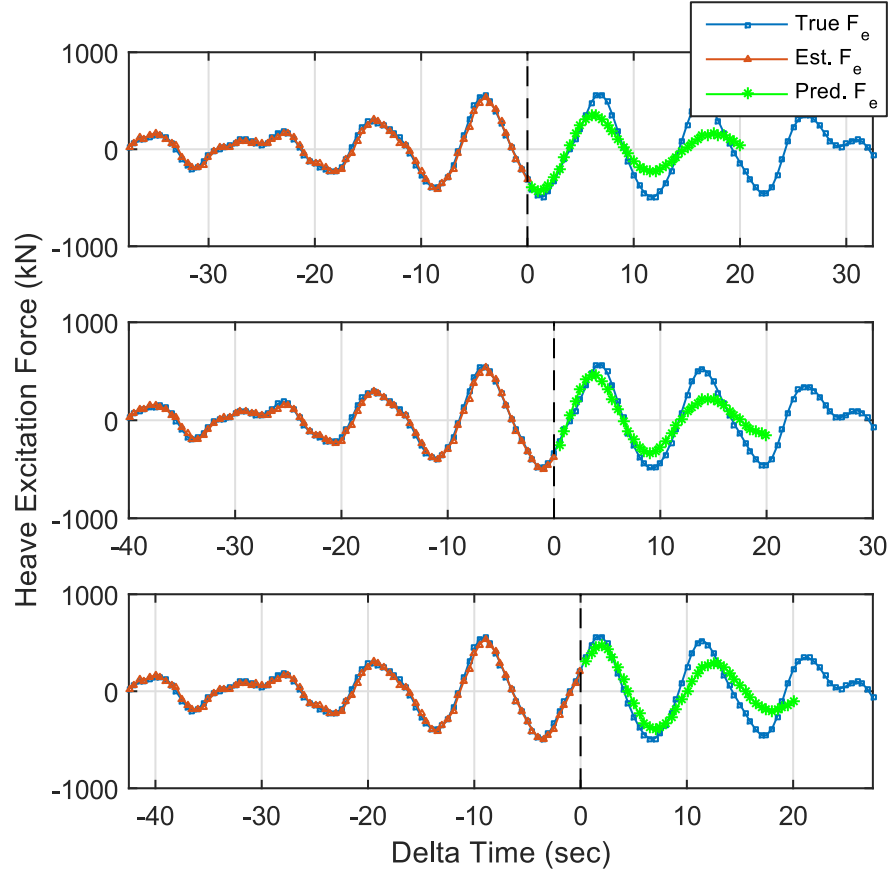
Figure 5.2: Three different snapshots in time illustrating the true excitation force, the estimated forces, and the predicted forces. The x axis represents delta time from the current time, so $t = 0$ in each plot is the current time, which is also indicated by the black dashed line. Each subplot is separated in time by 2.5 seconds.
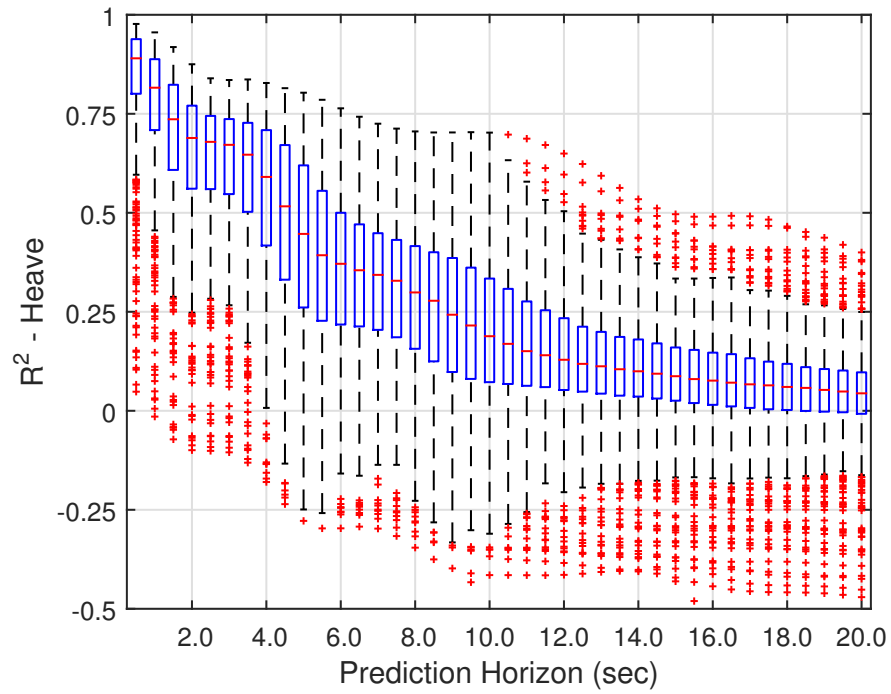
Figure 5.3: Heave excitation force prediction accuracy measured using correlation coefficient against the prediction horizon. At each prediction horizon the spread of performance across the sea states is shown using boxplots.

Figure 5.4: Surge excitation force prediction accuracy measured using correlation coefficient against the prediction horizon. At each prediction horizon the spread of performance across the sea states is shown using boxplots.

Figure 5.5: Pitch excitation force prediction accuracy measured using correlation coefficient against the prediction horizon. At each prediction horizon the spread of performance across the sea states is shown using boxplots.
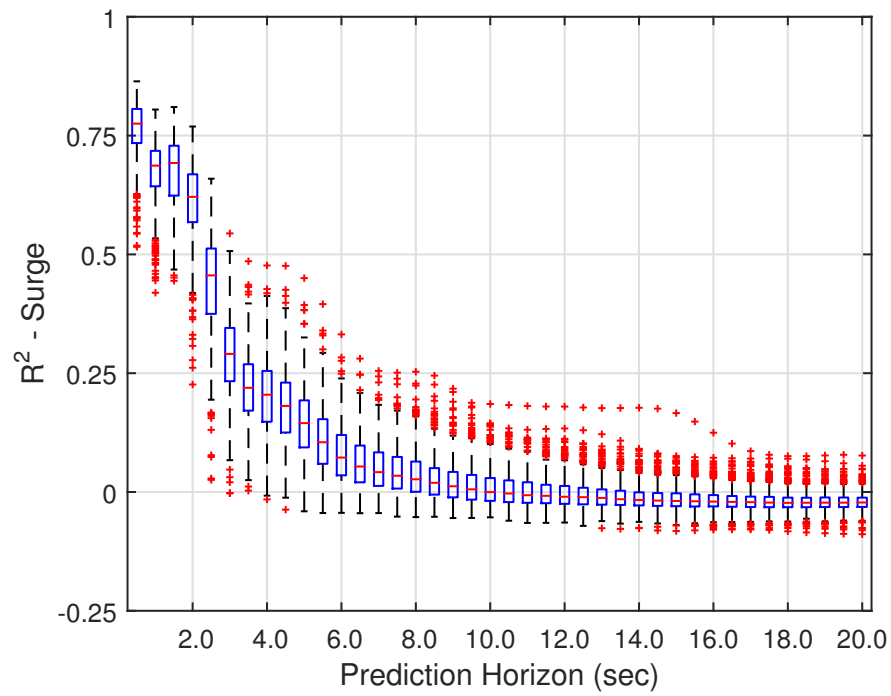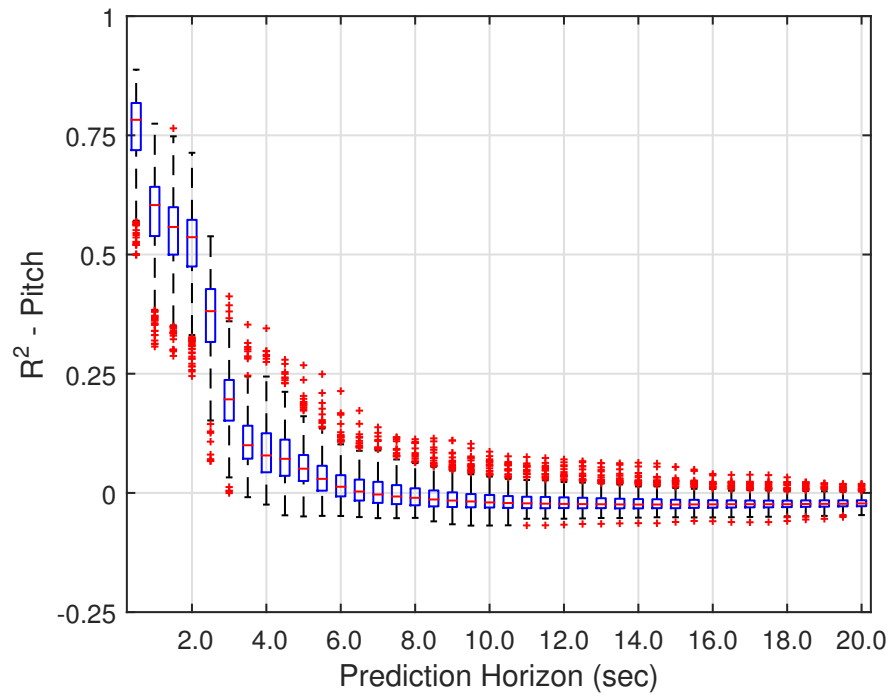
To test both of these hypotheses, first scatter plots of estimation performance and prediction performance are generated to see if there is a strong correlation between these two measures. These scatter plots, shown in Figure 5.6 are generated for each excitation force component, and at two different prediction horizons.
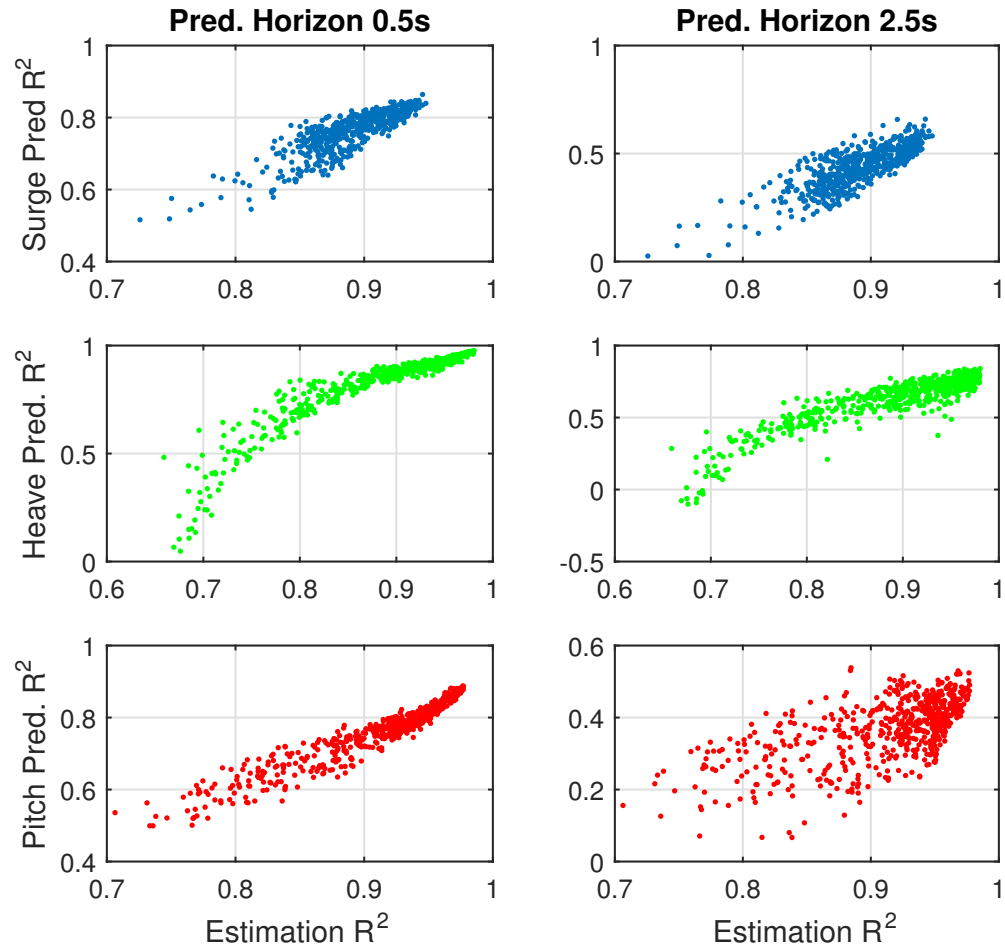

Figure 5.6: Scatter plot of prediction accuracy vs. estimation accuracy. Each row represents one of the force components, while the columns correspond to prediction horizons of 0.5 seconds and 2.5 seconds.

Inspection of Figure 5.6 shows that there is a relationship between estimation performance and prediction performance for all force components. A higher estimation accuracy results in higher prediction accuracies at both prediction horizons shown. This

suggests, but does not prove, that a reduction in estimation accuracy causes a reduction in prediction accuracy.

We take a closer look at this relationship by using the true excitation force values as inputs to the predictor, to visualize the effect using estimated force values has on prediction accuracy. This study was run on the four sea states used for training the estimators and predictors, shown in Figure 4.1. The prediction performance from each sea state is plotted separately as a scatter plot, shown in Figure 5.7.
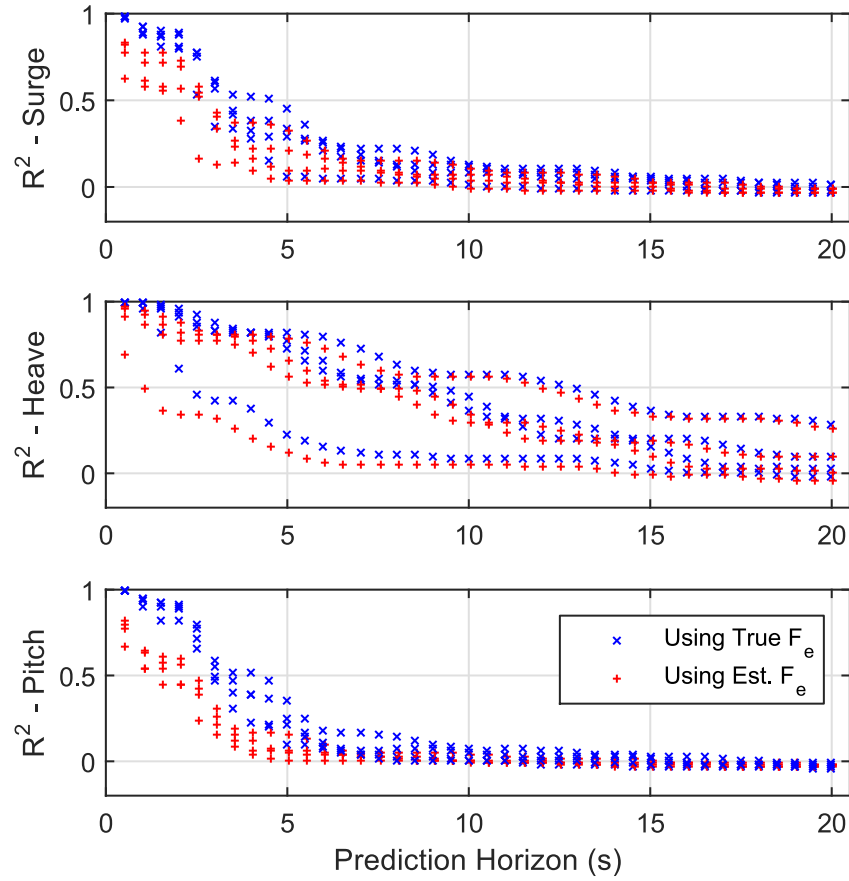

Figure 5.7: A comparison of prediction accuracy betwen using estimated excitation force values and true excitation force values as input to the recursive, autoregressive least square predictor. Results using true excitation force values are shown in blue, while results using estimated excitation force values are shown in red.

Figure 5.7 clearly shows that using the true force values as the input to the prediction algorithm results in higher accuracy predictions across all time horizons. Also worth nothing is the fact that even using true excitation force values for all three force components, the accuracy of the predictions in surge and pitch decrease more rapidly with prediction horizon than the heave force predictions. So while the estimation accuracy does reduce prediction accuracies for all force components, the shorter feasible prediction horizons in surge and pitch compared to heave cannot be fully explained by the reduced estimation accuracy in surge and pitch.

The cause of the reduced feasible prediction horizons in surge and pitch compared to heave is speculated to be the different frequency responses of the excitation force components. The bandpass frequency properties of the surge and pitch force components ensures the signal maintains higher frequency components then in heave, making predictions at longer prediction horizons more difficult.

Next the relationship between prediction accuracy and the bulk parameters of the sea states are investigated. The prediction performance is compared to the significant wave height and mean period of the sea state. Studies were also done comparing performance to other bulk statistics, including energy period and directional spreading, but no correlation was found, so these results are not presented. The comparisons were made by generating scatter plots of prediction performance correlation coefficients against the bulk sea state parameters. This was done for each excitation force component, at two prediction horizons. Prediction performance vs. mean period is shown in Figure 5.9, and prediction performance vs. significant wave height is shown in Figure 5.9.

Figure 5.8 shows a weak relationship between mean period and prediction horizon. Lower prediction accuracies happen much more often in sea states with short mean periods. This relationship is more pronounced for the heave force component then the surge and pitch force components. In surge and pitch, higher prediction accuracies at a horizon of 5.0 seconds occur most often at mean periods near 6.0 seconds.

Figure 5.9 shows a strong relationship between prediction accuracy as significant wave height, especially at a prediction horizon of 0.5 seconds. Almost all of the sea states with prediction correlation coefficients below 0.7 for all three force components occur when the significant wave height is below 2 meters. However, not all sea states with significant wave heights below 2 meters have poor prediction performances. This relationship, along with the weak relationship between prediction performance and mean
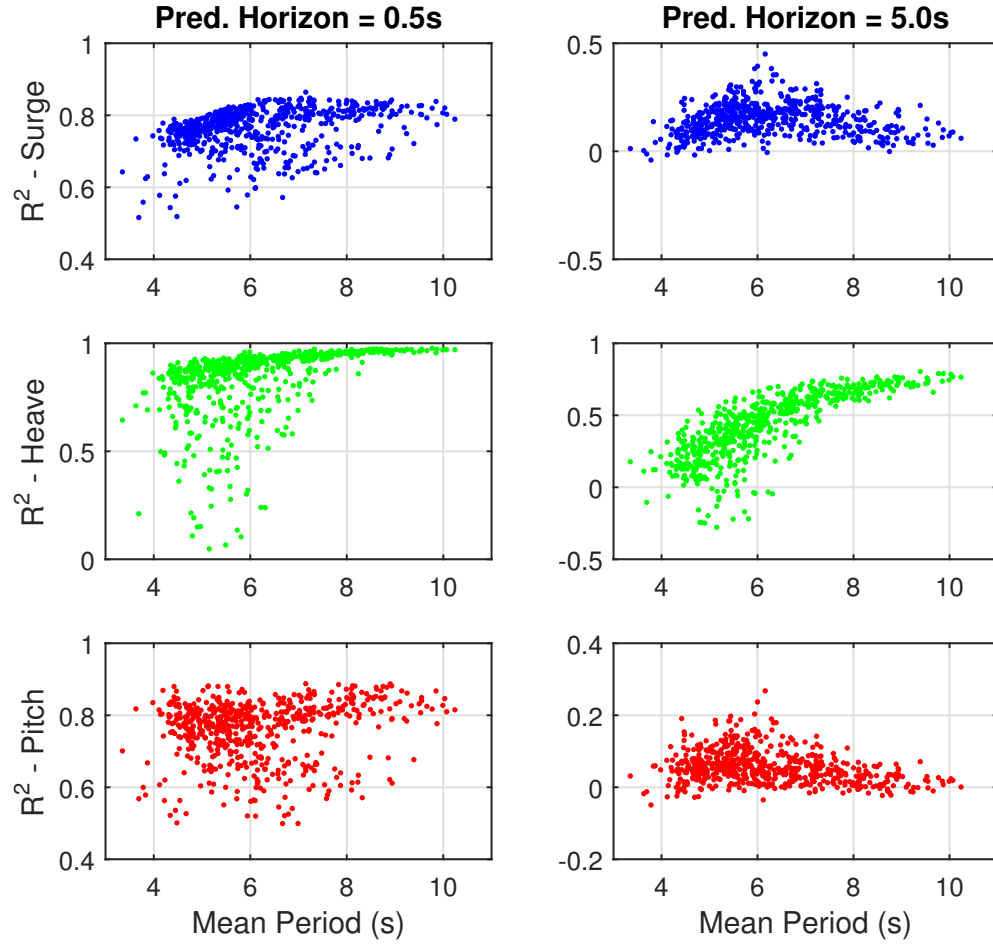
Figure 5.8: Prediction performance vs. mean wave period at prediction horizons of 0.5s and 5.0s. The first column of plots shows prediction accuracy at a horizon of 0.5s, and the second column of plots shows prediction accuracy at a horizon of 5.0s.

period, lead the author to speculate that low prediction performances are associated with sea states dominated by wind seas. The trends of prediction accuracy with respect to sea state parameters are similar to the trends observed between estimation accuracy and sea state parameters.
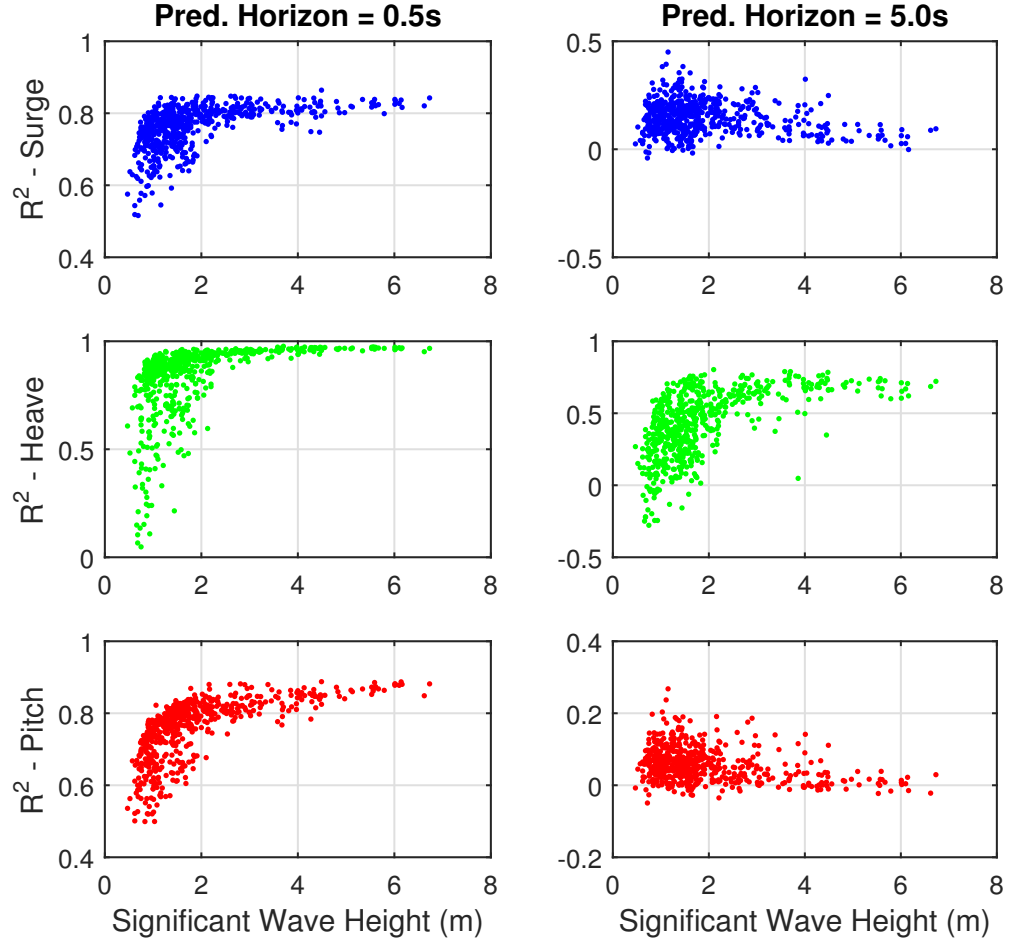
Figure 5.9: Prediction performance vs. significant wave height at prediction horizons of 0.5s and 5.0s. The first column of plots shows prediction accuracy at a horizon of 0.5s, and the second column of plots shows prediction accuracy at a horizon of 5.0s.

5.3 Discussion of Prediction Results

An adaptive wave excitation force predictor was developed in this section. The predictions are made with an autoregressive least squares prediction model, that is updated at each step to adapt to changing conditions. The number of regressors was selected by varying the number of regressors in the prediction model, and evaluating the performance on a small set of representative sea states. This showed a non-monotonic relationship

between the prediction performance and the number of regressors. The number of regressors was chosen to minimize the prediction error across the prediction horizon for all three force components. It is likely that the optimal number of regressors will depend on WEC design and site specific wave climates.

The performance of this predictor was then tested using 601 different sea states. It was shown that prediction accuracy is correlated with estimation accuracy. Prediction accuracy decreased at a faster rate with respect to prediction horizon for surge and pitch than it did in heave. This trend was also seen in a study done using true excitation force values as inputs to the prediction algorithm. This suggests the difference in possible prediction accuracies between force components is caused by the different frequency characteristics of the different excitation force components.

Benefits of using a recursive, autoregressive, least squares predictor include its ability to adapt to changing wave conditions, its low computational complexity, and its straightforward implementation. There is no requirement for a training data set that offline predictors require. While the specific accuracies presented here will depend on local wave climate and WEC design, this algorithm can be applied to any generic WEC that has the ability to estimate excitation forces.

Chapter 6: Conclusions

Most predictive control algorithms that are applied to WECs to increase average power output depend on having knowledge of the future wave excitation forces. Many authors neglect including how these predictions will be made available and instead simply assume full knowledge of future wave excitation forces.

The work presented in this thesis is a methodology that uses measurements of the WEC's position and velocity to estimate the excitation forces on the device, and then these estimated forces are used to predict future forces. This approach eliminates the need for additional wave measurement buoys or LIDAR to measure the approaching waves and propagate them forward. Instead of using a physics based prediction model, data driven time series prediction algorithms can be applied to generate predictions of the future excitation forces.

Various configurations of estimators were tested that involved different assumed disturbance models and different orders of radiation force approximations. The excitation forces were estimated using either a linear Kalman filter or an extended Kalman filter, depending on the configuration of the kalman prediction model. The process noise covariance matrices of each of these estimators was tuned to optimize estimation performance for all three excitation force components, in a range of different sea states. The best performing estimator for the WEC modeled had a 2nd order radiation force state space approximation, and am assumed harmonic oscillator disturbance model with an adaptive frequency.

The best performing estimator was then tested on 601 different recorded sea states to observe how different wave conditions would change estimation accuracy. For all three force components, estimation accuracy decreased significantly when the significant wave height of the recorded sea state was less than 2.0 meters. The hypothesis is that low energy wind seas have a higher degree of randomness than higher energy, swell dominated sea states, making estimating forces in these low energy conditions more challenging. However, this may not be a significant problem for wave energy applications as there is not much available energy in the sea states where estimation and performance accuracy

was poor.

A recursive, autoregressive least squares predictor was then developed. This prediction algorithm makes short term predictions using the estimated excitation forces generated by the Kalman filter estimators. The recursive nature of the predictor allows the model to adapt to changing wave conditions.

Tradeoff curves between order of the predictors and prediction accuracy were developed for a set of test sea states. This showed a non-monotonic relationship between number of regressors and prediction accuracy, so the number of regressors was chosen to maximize the prediction accuracy. The selected predictor was then tested on all 601 sea states, using the estimated excitation forces from the best performing estimator. Results showed that the prediction accuracy was closely correlated with estimation accuracy; lower estimation accuracy corresponded with lower prediction accuracy. Also observed is prediction accuracy as a function of prediction horizon decreased much more rapidly for surge and pitch than it did for heave. This is likely due to the differences in frequency response between heave and surge and pitch.

Using measurements of the WEC's motion to estimate excitation forces and then predict future forces provides a method that directly predicts the values needed by predictive controllers. Prediction of water surface elevation would require another intermediate step to calculate the excitation force from water surface elevation via convolution. This operation would require a longer prediction horizon due to the non-causality of the excitation force impulse response function. However, if prediction horizons longer than 10 seconds are needed, the time series methods will not be able to meet that prediction horizon requirement. Alternative methods involving upfield measurements of waves would have to be leveraged, to provide less accurate estimations over a longer time horizon.

While the estimator and predictor were developed and tested using recorded water surface elevation data, the WEC model is an analytic model. In developing the estimators and predictors presented here, we had the luxury of knowing what the true excitation force values are. This luxury will not exist for a physical WEC in a wave tank or deployed at sea, so other approaches will have to be taken to tune the estimator and predictor algorithms. One approach would be to develop a dynamic model for the WEC, experimentally validate its performance, and then follow the process outlined in this thesis for developing the predictors and estimators. The experimentally validated WEC model would be used to gage the performance of the estimators and predictors.

Other potential future work includes expanding the recursive, autoregressive least squares predictor to have an exogenous input. Different exogenous inputs could be tested, perhaps a filtered version of the estimated excitation force or time series that are derived from current sea state bulk data or spectral data. A more mathematically refined method of tuning the process noise covariance matrices could also be developed, potentially improving estimation accuracy. There has been some research in using an autocovariance least squares method of identifying the process noise covariance matrix that may yield higher accuracy excitation force estimations [32]. Another potential approach to improve both estimation and prediction accuracy would be to have different estimators and predictors tuned for different sea states, and then switch between these configurations based on the present sea state characteristics.

Bibliography

[1] Jacobson, P., 2011. Mapping and assessment of the united states ocean wave energy resource. Final Report 1024637, Electric Power Research Institute (EPRI), Palo Alto, CA, December. See also URL `http://www.abc.edu`.

[2] Garcìa-Medina, G., Özkan-Haller, H. T., Ruggiero, P., and Oskamp, J., 2013. "An Inner-Shelf Wave Forecasting System for the U.S. Pacific Northwest". *Weather and Forecasting,* **28**(3), February, pp. 681–703.

[3] Smith, D., 2005. "Why wave, tide and ocean current promise more than wind.". *Modern Power Systems,* **25**(5), June, pp. 47–53.

[4] Brekken, T., 2011. "On Model Predictive Control for a point absorber Wave Energy Converter". In PowerTech, 2011 IEEE Trondheim, pp. 1–8.

[5] Li, G., Weiss, G., Mueller, M., Townley, S., and Belmont, M. R., 2012. "Wave energy converter control by wave prediction and dynamic programming". *Renewable Energy,* **48**(0), pp. 392 – 403.

[6] Hals, J., Falnes, J., and Moan, T., 2011. "A Comparison of Selected Strategies for Adaptive Control of Wave Energy Converters". *Journal of Offshore Mechanics and Arctic Engineering,* **133**(3), Mar., p. 031101.

[7] Falnes, J., 2002. *Ocean waves and oscillating systems: linear interactions including wave-energy extraction.* Cambridge University Press.

[8] Falnes, J., and Budal, K., 1978. "Wave-power absorption by point absorbers". *Norwegian Maritime Research,* **6**, pp. 2–11.

[9] Richter, M., Magana, M., Sawodny, O., and Brekken, T., 2013. "Nonlinear Model Predictive Control of a Point Absorber Wave Energy Converter". *IEEE Transactions on Sustainable Energy,* **4**(1), pp. 118–126.

[10] Tom, N., and Yeung, R. W., 2014. "Nonlinear Model Predictive Control Applied to a Generic Ocean-Wave Energy Extractor". *Journal of Offshore Mechanics and Arctic Engineering,* **136**(4), July, p. 041901.

[11] Abraham, E., and Kerrigan, E., 2013. "Optimal Active Control and Optimization of a Wave Energy Converter". *IEEE Transactions on Sustainable Energy,* **4**(2), Apr., pp. 324–332.

[12] Schoen, M., Hals, J., and Moan, T., 2011. "Wave Prediction and Robust Control of Heaving Wave Energy Devices for Irregular Waves". *IEEE Transactions on Energy Conversion,* **26**(2), pp. 627–638.

[13] Scruggs, J., Lattanzio, S., Taflanidis, A., and Cassidy, I., 2013. "Optimal causal control of a wave energy converter in a random sea". *Applied Ocean Research,* **42**, Aug., pp. 1–15.

[14] Belmont, M. R., Horwood, J. M. K., Thurley, R. W. F., and Baker, J., 2006. "Filters for linear sea-wave prediction". *Ocean Engineering,* **33**(1718), Dec., pp. 2332–2351.

[15] Belmont, M. R., and Ashwin, P., 2011. "The Independent Variable Interpolation Technique for Nonuniformly Sampled Shallow-Angle Lidar Data". *Journal of Atmospheric and Oceanic Technology,* **28**(12), Aug., pp. 1672–1678.

[16] Belmont, M. R., Horwood, J. M. K., Thurley, R. W. F., and Baker, J., 2007. "Shallow Angle Wave Profiling Lidar". *Journal of Atmospheric and Oceanic Technology,* **24**(6), June, pp. 1150–1156.

[17] Belmont, M. R., Christmas, J., Dannenberg, J., Hilmer, T., Duncan, J., Duncan, J. M., and Ferrier, B., 2014. "An Examination of the Feasibility of Linear Deterministic Sea Wave Prediction in Multidirectional Seas Using Wave Profiling Radar: Theory, Simulation, and Sea Trials". *Journal of Atmospheric and Oceanic Technology,* **31**(7), Apr., pp. 1601–1614.

[18] Halliday, J. R., Dorrell, D. G., and Wood, A. R., 2011. "An application of the Fast Fourier Transform to the short-term prediction of sea wave behaviour". *Renewable Energy,* **36**(6), June, pp. 1685–1692.

[19] Cahill, B., and Lewis, A., 2010. "Wavelet analysis applied to the wave energy resource at an irish west coast site". In OCEANS 2010, pp. 1–7.

[20] Fusco, F., and Ringwood, J., 2009. "A Study on Short-Term Sea Profile Prediction for Wave Energy Applications". In Proceedings of the 8th European Wave and Tidal Energy Conference, pp. 756–765.

[21] Fusco, F., and Ringwood, J., 2010. "Short-Term Wave Forecasting for Real-Time Control of Wave Energy Converters". *IEEE Transactions on Sustainable Energy,* **1**(2), July, pp. 99–106.

[22] Boren, B., Ling, B., Batten, B., and Paasch, R., 2014. "Using Artificial Neural Networks for Prompt and Accurate Wave Prediction at Northwest National Marine Renewable Energy Center's North Energy Test Site: a Feasibility Analysis". In Grand Renewable Energy 2014 Proceedings.

[23] Cummins, W. E., 1962. The impulse response function and ship motions. Technical Report 1661, Department of the Navy, October.

[24] ANSYS, I., 2014. ANSYS Aqwa v14.0. URL `www.ansys.com`.

[25] Yu, Z., and Falnes, J., 1995. "State-space modelling of a vertical cylinder in heave". *Applied Ocean Research,* **17**(5), Oct., pp. 265–275.

[26] Kristiansen, E., Hjulstad, s., and Egeland, O., 2005. "State-space representation of radiation forces in time-domain vessel models". *Ocean Engineering,* **32**(1718), Dec., pp. 2195–2216.

[27] Kung, S., 1978. "A New Identification and Model Reduction Algorithm via Singular Value Decompositions". In Proceedings of the Twelfth Asilomar Conference and Circuits, Systems and Computers, pp. 705–714.

[28] Brekken, T., von Jouanne, A., and Han, H. Y., 2009. "Ocean wave energy overview and research at Oregon State University". In Power Electronics and Machines in Wind Applications, 2009. PEMWA 2009. IEEE, pp. 1–7.

[29] Dan Simon, 2006. *Optimal State Estimation*, 1st ed. John Wiley & Sons, Hoboken, NJ.

[30] Falnes, J., 1995. "On non-causal impulse response functions related to propagating water waves". *Applied Ocean Research,* **17**(6), Dec., pp. 379–389.

[31] Ljung, L., 1987. *System identification: Theory for the user*, 1st ed. Prentice-Hall, Inc., Englewood Cliffs, New Jersey.

[32] Rajamani, M. R., and Rawlings, J. B., 2009. "Estimation of the disturbance structure from data using semidefinite programming and optimal weighting". *Automatica,* **45**(1), Jan., pp. 142–148.